



THE UNIVERSITY *of* EDINBURGH

Edinburgh Research Explorer

SPOCD1 is an essential executor of piRNA-directed 1 de novo DNA methylation

Citation for published version:

Zoch, A, Auchynnikava, T, Berrens, RV, Kabayama, Y, Schöpp, T, Heep, M, Vasiliauskait, L, Pérez-Rico, YA, Cook, AG, Shkumatava, A, Rappsilber, J, Allshire, RC & O'Carroll, D 2020, 'SPOCD1 is an essential executor of piRNA-directed 1 de novo DNA methylation', *Nature*, vol. 584, no. 7822, pp. 635-639.
<https://doi.org/10.1038/s41586-020-2557-5>

Digital Object Identifier (DOI):

[10.1038/s41586-020-2557-5](https://doi.org/10.1038/s41586-020-2557-5)

Link:

[Link to publication record in Edinburgh Research Explorer](#)

Document Version:

Peer reviewed version

Published In:

Nature

Publisher Rights Statement:

This is the accepted version of the following article: Zoch, A., Auchynnikava, T., Berrens, R.V. et al. SPOCD1 is an essential executor of piRNA-directed de novo DNA methylation. *Nature* (2020).
<https://doi.org/10.1038/s41586-020-2557-5>, which has been published in final form at
<https://www.nature.com/articles/s41586-020-2557-5>.

General rights

Copyright for the publications made accessible via the Edinburgh Research Explorer is retained by the author(s) and / or other copyright owners and it is a condition of accessing these publications that users recognise and abide by the legal requirements associated with these rights.

Take down policy

The University of Edinburgh has made every reasonable effort to ensure that Edinburgh Research Explorer content complies with UK legislation. If you believe that the public display of this file breaches copyright please contact openaccess@ed.ac.uk providing details, and we will remove access to the work immediately and investigate your claim.



1 **SPOCD1 is an essential executor of piRNA-directed *de novo* DNA methylation**

2

3 Ansgar Zoch^{1,2}, #Tania Auchynnikava², #Rebecca V. Berrens³, #Yuka Kabayama^{1,2}, Theresa
4 Schöpp^{1,2}, Madeleine Heep^{1,2}, Lina Vasiliauskaitė¹, Yuvia A. Pérez-Rico⁴, Atlanta G. Cook²,
5 Alena Shkumatava⁴, Juri Rappsilber^{2,5}, Robin C. Allshire² and *Dónal O'Carroll^{1,2}

6

7 1. MRC Centre for Regenerative Medicine, Institute for Stem Cell Research, School of
8 Biological Sciences, University of Edinburgh, 5 Little France Drive, Edinburgh, EH16
9 4UU, UK.

10 2. Wellcome Centre for Cell Biology, University of Edinburgh, Edinburgh, EH9 3BF,
11 UK.

12 3. Cancer Research UK Cambridge Institute, University of Cambridge, Li Ka Shing
13 Centre, Robinson Way, Cambridge, CB2 0RE, UK.

14 4. Institut Curie, PSL Research University, CNRS UMR 3215, INSERM U934, 26 rue
15 d'Ulm, 75248 Paris, France.

16 5. Institute of Biotechnology, Technische Universität Berlin, Berlin, Germany.

17

18 #These authors contributed equally to this work.

19 *Corresponding author: Dónal O'Carroll (donal.ocarroll@ed.ac.uk)

20

21

22 **In mammals, the acquisition of the germline from the soma provides the germline with**
23 **an essential challenge, the necessity to erase and reset genomic methylation¹. In the male**
24 **germline RNA-directed DNA methylation silences young active transposable elements**
25 **(TEs)²⁻⁴. The PIWI protein MIWI2 (PIWIL4) and its associated PIWI-interacting RNAs**
26 **(piRNAs) instruct TE DNA methylation^{3,5}. PiRNAs are proposed to tether MIWI2 to**
27 **nascent TE transcripts, however the mechanism by which MIWI2 directs *de novo* TE**
28 **methylation is poorly understood but central to the immortality of the germline. Here, we**
29 **define the interactome of MIWI2 in foetal gonocytes that are undergoing *de novo* genome**
30 **methylation and identify a novel MIWI2-associated factor, SPOCD1, that is essential for**
31 **young TE methylation and silencing. The loss of *Spocd1* in mice results in male-specific**
32 **infertility but impacts neither piRNA biogenesis nor localization of MIWI2 to the nucleus.**
33 **SPOCD1 is a nuclear protein and its expression is restricted to the period of *de novo***
34 **genome methylation. We found SPOCD1 co-purified *in vivo* with DNMT3L and**
35 **DNMT3A, components of the *de novo* methylation machinery as well as constituents of**
36 **the NURD and BAF chromatin remodelling complexes. We propose a model whereby**
37 **tethering of MIWI2 to a nascent TE transcript recruits repressive chromatin remodelling**
38 **activities and the *de novo* methylation apparatus through SPOCD1. In summary, we have**
39 **identified a novel and essential executor of mammalian piRNA-directed DNA**
40 **methylation.**

41

42 The germline gives rise to the sperm and egg cells that are the basis of reproduction and
43 heredity. One of the biggest threats to the integrity of the germline are TEs that have the ability
44 to cause mutation through transposition. In mammals, DNA methylation is an important
45 determinant of TEs silencing⁶. The mammalian germline is derived from somatic cells early
46 during development⁷ and this acquisition from the soma necessitates the process of germline

47 reprogramming and *de novo* genome methylation to reset genomic DNA methylation patterns¹.
48 In the mouse male germline, the process of *de novo* DNA methylation occurs in gonocytes
49 mostly during embryonic development^{4,6}. DNMT3L is the key mediator of genome
50 methylation that interacts with and stimulates the DNMT3 (DNMT3A, DNMT3B and
51 DNMT3C) *de novo* DNA methyltransferases⁸⁻¹³. DNMT3A and DNMT3B may act
52 redundantly on TEs during *de novo* genome methylation whereas the rodent-specific DNMT3C
53 has a specialized function in TE methylation¹²⁻¹⁵. The first wave of *de novo* methylation is
54 indiscriminate leading to the bulk genomic methylation⁴. Many active long interspersed nuclear
55 element-1 (LINE1) and intracisternal A-particle (IAP) copies escape the first round of
56 methylation and remain expressed, threatening the genomic integrity of the germline⁴. The
57 PIWI proteins and their associated small non-coding PIWI-interacting RNA (piRNAs)
58 eliminate this threat through post-transcriptional and transcriptional silencing mechanisms¹⁶.
59 The PIWI protein MILI (PIWIL2) destroys cytoplasmic TE transcripts by piRNA-guided
60 endonucleolytic cleavage that leads to the initiation of effector piRNA production¹⁷. The
61 resulting effector piRNAs are proposed to guide the nuclear PIWI protein MIWI2 to active TE
62 loci by tethering the ribonucleoprotein particle to the nascent transcript and instructing DNA
63 methylation by an unknown mechanism¹⁶.

64 To explore the mechanism of piRNA-instructed *de novo* DNA methylation, we employed a
65 proteomics approach using our *Miwi2^{HA}* allele¹⁸ that encodes an endogenously expressed fully
66 functional N-terminal epitope-tagged HA-MIWI2 and performed anti-HA
67 immunoprecipitation coupled with quantitative mass spectrometry (IP-MS) from extracts of
68 *Miwi2^{+/+}* (negative control) and *Miwi2^{HA/HA}* embryonic day 16.5 (E16.5) foetal testes (Fig. 1a,
69 Supplementary Data Table 1). This approach identified 28 MIWI2-associated proteins
70 (enrichment >4-fold, P<0.05). Encouragingly, 12 of these have been implicated in piRNA
71 biogenesis¹⁶ with 5 being novel MIWI2 interactors (Fig. 1b). We also identified 16 additional

72 (14 novel) interacting proteins (Fig. 1b) that could either participate in piRNA biogenesis
73 (cytoplasmic) or nuclear MIWI2 functions. To identify nuclear factors required for the
74 execution of MIWI2 function, we applied the following criteria. First, the expression of the
75 gene should be restricted to the period of *de novo* genome methylation as is the case for *Miwi2*
76 and *Dnmt3l* (Fig. 1c and Extended Data Fig. 1a). This criterion would likely exclude novel
77 piRNA biogenesis factors as they would be expected to be expressed also in adult
78 spermatogenic populations, as exemplified by *Mili* (*Piwil2*) and *Vasa* (*Ddx4*) (Fig. 1c and
79 Extended Data Fig. 1a). Second, the gene should encode a protein with a nuclear localization
80 signal (NLS). Applying these criteria, we found a single gene *Spocd1* (Fig. 1c and Extended
81 Data Fig. 1b) of unknown function that encodes for a 1015 amino acid protein with a TFIIS-M
82 domain and a SPOC domain (Fig. 1d). Intriguingly, a SPOC domain previously described in
83 SHARP (SPEN, MINT) has been shown to recruit the transcriptional co-repressor
84 NCoR/SMRT^{19,20}. The SPOC domain of SPOCD1 is closely related to the one found in PHF3
85 and DIDO1; and both of these proteins also contain a TFIIS-M domain (Extended Data Fig.
86 2a-b). Indeed, phylogenetic analysis supports that *Spocd1* originated from a duplication of *Phf3*
87 in the common ancestor of lobe-finned fishes and tetrapods (Extended Data Fig. 3). In
88 summary, we have identified SPOCD1 as a MIWI2 interactor that is a strong candidate for a
89 facilitator of nuclear MIWI2 function.

90 The loss of piRNA-pathway factors or the *de novo* DNA methylation machinery results in male
91 infertility, arrested spermatogenesis in meiosis and deregulation of LINE1 and IAP elements
92 in mice^{2,3,5,9,12,13,17,21}. To explore a potential role for SPOCD1 in the piRNA pathway, we
93 generated a mutant allele (*Spocd1*⁻) in the mouse (Extended Data Fig. 4a-c). *Spocd1*-deficiency
94 resulted in male-specific infertility with the complete absence of spermatozoa in the epididymis
95 (Fig. 2a, b and Extended Data Fig. 4d). The testes of *Spocd1*⁻ mice were atrophic (Fig. 2c);
96 histological analyses of *Spocd1*⁻ testis revealed aberrant seminiferous tubules that lacked

97 spermatids and presented a meiotic arrest at the early pachytene stage (Fig. 2d and Extended
98 Data Fig. 4e). In addition, chromosome pairing is defective in *Spocd1*^{-/-} meiotic cells (Extended
99 Data Fig. 4f), a hallmark of mutations that result in LINE1 derepression⁹. The expression of
100 LINE1 and IAP were both detected in the seminiferous tubules of adult *Spocd1*^{-/-} testis (Fig.
101 2e, f). To explore the full repertoire of deregulated TEs, we performed RNA-seq that revealed
102 that the same families of TEs are deregulated in post-natal day 20 (P20) testis of *Miwi2*^{-/-} or
103 *Spocd1*^{-/-} mice (Fig. 2g and Extended Data Fig. 4g-i). Phosphorylation of the histone variant
104 H2AX (γ H2AX) is a marker of double stranded breaks²²; staining of testis sections revealed
105 the characteristic foci observed in meiotic cells in *Spocd1*^{+/+} mice whereas a strong γ H2AX
106 stain indicative of extensive DNA damage was observed in *Spocd1*^{-/-} meiocytes (Fig. 2h).
107 Indeed, widespread apoptosis of meiotic cells was observed in *Spocd1*^{-/-} testes (Fig. 2i). In
108 summary, SPOCD1 is essential for spermatogenesis and is required for transposon repression.
109 The piRNA pathway is required for *de novo* DNA methylation of IAP elements and several
110 sub-families of LINE1²⁻⁵. We next sought to determine if SPOCD1 is required for piRNA-
111 directed *de novo* DNA methylation. We thus isolated genomic DNA from wildtype, *Spocd1*^{-/-}
112 and *Miwi2*^{-/-} P14 spermatogonia and performed whole genome methylation sequencing
113 (Methyl-seq). We choose this time point as it is after completion of *de novo* genome
114 methylation, prior to the onset of *Spocd1*^{-/-} phenotypic defects with SPOCD1. Indeed, no major
115 changes in methylation in *Spocd1*^{-/-} spermatogonia were observed in genic, intergenic, CpG
116 island or promoter regions (Fig. 3a and Extended Data Fig. 5a,b). Globally, *Spocd1*-deficiency
117 did not affect collective transposon (all TEs grouped) methylation levels (Fig. 3a and Extended
118 Data Fig. 5a,b). Consistent with *Miwi2*-deficiency, IAPEy and MMERVK10C as well as the
119 young LINE1 families L1Md_A, L1Md_T and L1Md_Gf failed to be fully methylated in
120 *Spocd1*^{-/-} spermatogonia (Fig. 3b and Extended Data Fig. 5c,d). Metaplot analysis demonstrated
121 defective *de novo* methylation specifically at TE promotor elements in *Spocd1*^{-/-} spermatogonia

122 (Fig. 3c and Extended Data Fig. 6a), which is a hallmark of piRNA- and DNMT3C- directed
123 methylation (Extended Data Fig. 6b)^{12,23}. The loss of methylation was particularly evident in
124 young LINE1 families and elements such as L1Md_T and L1Md_Gf compared to the older
125 L1Md_F (Fig. 3c-d and Extended Data Fig. 6c). MIWI2 is required specifically for the
126 methylation of one imprinted locus, *Rasgrfl*²⁴. Consistently, among imprinted loci, only
127 *Rasgrfl* methylation is dependent upon SPOCD1 function (Fig. 3e). In summary, SPOCD1 is
128 required for *de novo* DNA methylation of the TEs that are regulated by the piRNA pathway.
129 The dependency of piRNA-mediated silencing of TEs on SPOCD1 may indicate a role for
130 SPOCD1 as a downstream effector of nuclear MIWI2 function or alternatively in piRNA
131 biogenesis, amplification or loading; as mutations that disrupt these processes will lead to the
132 same phenotypic outcome. We therefore sequenced small RNA from *Spocdl*^{+/-} and *Spocdl*^{-/-}
133 E16.5 foetal testes to analyse piRNA biogenesis. We found no major impact of *Spocdl*-
134 deficiency on length distribution (Fig. 3f), annotation of mapped piRNAs (Fig. 3g and
135 Extended Data Fig. 7a), relative piRNA counts (Extended Data Fig. 7b), piRNA amplification
136 (Fig. 3h Extended Data Fig. 7c-e) or piRNAs mapping to TEs (Extended Data Fig. 7f). piRNA
137 binding to MIWI2 licences its entry to the nucleus, thus disruption of piRNA biogenesis,
138 amplification or loading results in the dramatic reduction of MIWI2's nuclear
139 localization^{17,18,25}. The fact that MIWI2 exhibits normal localization in the absence of *Spocdl*
140 (Fig. 3i) confirms that SPOCD1 is not required for piRNA processing but suggests its
141 involvement in the execution of MIWI2's nuclear function. A possible alternative nuclear
142 function could be that SPOCD1 acts as transcription factor required for either transposon or
143 gene expression. However, RNA-seq from E16.5 foetal gonocytes revealed *Spocdl*-deficiency
144 had a minimal impact on gene expression and normal expression for the majority of TEs but,
145 importantly, the piRNA-regulated TEs were mostly expressed at or above normal levels in
146 *Spocdl*^{-/-} E16.5 foetal gonocytes (Extended Data Fig. 8a-b, Supplementary Data Table 2 and

147 3). Collectively, these data are not supportive of a role for SPOCD1 as a transcription or a
148 piRNA biogenesis factor.

149 We next sought to explore how SPOCD1 contributes to *de novo* TE methylation. We thus
150 engineered the *Spocd1^{HA}* allele where the sequence encoding the HA epitope tag has been
151 inserted into the *Spocd1* locus to generate an endogenously expressed, fully functional C-
152 terminal epitope-tagged SPOCD1-HA (Fig. 4a and Extended Data Fig. 9a-d). Confocal
153 immunolocalization of SPOCD1-HA on E16.5 foetal testis sections revealed that SPOCD1 is
154 restricted to foetal gonocytes and predominantly nuclear (Fig. 4b). Furthermore, SPOCD1
155 expression is restricted to the period of *de novo* DNA methylation (Fig. 4c and Extended Data
156 Fig. 9e-f). Expression of SPOCD1 commenced at E14.5 preceding MIWI2 expression by a day
157 with expression of both proteins extinguished by P5 (Fig. 4c, d and Extended Data Fig. 9e-g).
158 To explore how SPOCD1 might mediate *de novo* DNA methylation we performed anti-HA IP-
159 MS from extracts of *Spocd1^{+/+}* (negative control) and *Spocd1^{HA/+}* E16.5 foetal testes (Fig 4e, f,
160 Supplementary Data Table 4). We identified 72 proteins (enrichment >4-fold, P<0.05) that
161 associate with SPOCD1-HA, amongst which were DNMT3L and DNMT3A, components of
162 the *de novo* methylation machinery (Fig 4e, f, Supplementary Data Table 4). A few peptides
163 corresponding to DNMT3C were detected in the SPOCD1 precipitates, but their abundance
164 was insufficient to meet our stringent co-purification criteria. We confirmed the co-
165 precipitation of SPOCD1 with components of the *de novo* methylation machinery using HEK
166 cells as an orthologous system (Extended Data Fig. 10). Several components of the repressive
167 chromatin remodelling NURD and BAF complexes co-purified with SPOCD1 (Fig 4e, f,
168 Supplementary Data Table 4). At least one paralogue of all components of the core NURD
169 complex bar one²⁶ and several of the BAF complex²⁷ were enriched in SPOCD1 IPs (Fig 4e, f,
170 Supplementary Data Table 4). We also found MIWI2 significantly enriched in the SPOCD1 IP
171 but less than the stringent 4-fold cut off (P<0.011, 1.9-fold enriched). We noted a poor overlap

172 between the factors co-precipitated by MIWI2 and SPOCD1, which could arise from different
173 extraction procedures between the respective IPs. We re-performed MIWI2 IP-MS but
174 included Benzonase to aid chromatin solubilization, as was done in the SPOCD1 IP-MS
175 experiment. This revealed a major overlap in co-precipitated proteins between MIWI2 and
176 SPOCD1 (Fig 4g, h, Supplementary Data Table 5). Importantly, the interaction with SPOCD1
177 was confirmed and we now found NURD (MTA3) and BAF (ARID1A and SMARCA5)
178 components in the MIWI2 IP using the same stringent association criteria (enrichment >4-fold,
179 $P < 0.05$). Moreover, we also found DNMT3L as well as additional BAF and NURD
180 components significantly enriched (<4-fold) in the MIWI2 IP (Supplementary Data Table 6).
181 In summary, we have shown that SPOCD1 is a nuclear protein, specifically expressed during
182 the period of *de novo* DNA methylation and co-precipitates the *de novo* DNA methylation
183 machinery as well as several chromatin remodelling complexes.

184 Here we have defined MIWI2-associated factors in E16.5 foetal gonocytes; among these we
185 have identified SPOCD1 and shown its requirement for piRNA-directed TE methylation.
186 While SPOCD1 robustly co-purified with MIWI2, we did not observe MIWI2 in SPOCD1
187 immunoprecipitates within the stringent high enrichment and confidence interactors. We
188 interpret this observation as indicating that only a fraction of SPOCD1 is bound either directly
189 or indirectly to MIWI2. This fraction likely merits the portion of MIWI2 that has identified an
190 active TE and engaged in silencing. Indeed, it may be important to uncouple MIWI2 from the
191 effector machinery until a *bona fide* target has been identified to avoid precocious aberrant
192 methylation and possible epimutations that would be transmitted to the next generation. We
193 propose a tentative model of MIWI2-piRNA directed DNA methylation whereby high
194 complementarity base pairing of the piRNA to a nascent TE transcript licences MIWI2 to
195 engage SPOCD1 and the associated chromatin remodelling and DNA methylation machinery.

196 In conclusion, we have identified SPOCD1 as an essential nuclear effector of MIWI2 function
197 and provide the first mechanistic insights into mammalian piRNA-directed methylation.

198

199 **Methods summary**

200 Full Methods and any associated references are available in the online version of the paper at
201 www.nature.com/nature.

202

203 **References**

204

205 1 Tang, W. W., Kobayashi, T., Irie, N., Dietmann, S. & Surani, M. A. Specification and
206 epigenetic programming of the human germ line. *Nat Rev Genet* **17**, 585-600,
207 doi:10.1038/nrg.2016.88 (2016).

208 2 Aravin, A. A., Sachidanandam, R., Girard, A., Fejes-Toth, K. & Hannon, G. J.
209 Developmentally regulated piRNA clusters implicate MILI in transposon control.
210 *Science* **316**, 744-747, doi:10.1126/science.1142612 (2007).

211 3 Carmell, M. A. *et al.* MIWI2 is essential for spermatogenesis and repression of
212 transposons in the mouse male germline. *Dev Cell* **12**, 503-514,
213 doi:10.1016/j.devcel.2007.03.001 (2007).

214 4 Molaro, A. *et al.* Two waves of de novo methylation during mouse germ cell
215 development. *Genes Dev* **28**, 1544-1549, doi:10.1101/gad.244350.114 (2014).

216 5 Kuramochi-Miyagawa, S. *et al.* DNA methylation of retrotransposon genes is regulated
217 by Piwi family members MILI and MIWI2 in murine fetal testes. *Genes Dev* **22**, 908-
218 917, doi:10.1101/gad.1640708 (2008).

- 219 6 Walsh, C. P., Chaillet, J. R. & Bestor, T. H. Transcription of IAP endogenous
220 retroviruses is constrained by cytosine methylation. *Nat Genet* **20**, 116-117,
221 doi:10.1038/2413 (1998).
- 222 7 Ohinata, Y. *et al.* Blimp1 is a critical determinant of the germ cell lineage in mice.
223 *Nature* **436**, 207-213, doi:10.1038/nature03813 (2005).
- 224 8 Chedin, F., Lieber, M. R. & Hsieh, C. L. The DNA methyltransferase-like protein
225 DNMT3L stimulates de novo methylation by Dnmt3a. *Proc Natl Acad Sci U S A* **99**,
226 16916-16921, doi:10.1073/pnas.262443999 (2002).
- 227 9 Bourc'his, D. & Bestor, T. H. Meiotic catastrophe and retrotransposon reactivation in
228 male germ cells lacking Dnmt3L. *Nature* **431**, 96-99, doi:10.1038/nature02886 (2004).
- 229 10 Suetake, I., Shinozaki, F., Miyagawa, J., Takeshima, H. & Tajima, S. DNMT3L
230 stimulates the DNA methylation activity of Dnmt3a and Dnmt3b through a direct
231 interaction. *J Biol Chem* **279**, 27816-27823, doi:10.1074/jbc.M400181200 (2004).
- 232 11 Webster, K. E. *et al.* Meiotic and epigenetic defects in Dnmt3L-knockout mouse
233 spermatogenesis. *Proc Natl Acad Sci U S A* **102**, 4068-4073,
234 doi:10.1073/pnas.0500702102 (2005).
- 235 12 Barau, J. *et al.* The DNA methyltransferase DNMT3C protects male germ cells from
236 transposon activity. *Science* **354**, 909-912, doi:10.1126/science.aah5143 (2016).
- 237 13 Jain, D. *et al.* rahu is a mutant allele of Dnmt3c, encoding a DNA methyltransferase
238 homolog required for meiosis and transposon repression in the mouse male germline.
239 *PLoS Genet* **13**, e1006964, doi:10.1371/journal.pgen.1006964 (2017).
- 240 14 Kaneda, M. *et al.* Essential role for de novo DNA methyltransferase Dnmt3a in paternal
241 and maternal imprinting. *Nature* **429**, 900-903, doi:10.1038/nature02633 (2004).

- 242 15 Kato, Y. *et al.* Role of the Dnmt3 family in de novo methylation of imprinted and
243 repetitive sequences during male germ cell development in the mouse. *Hum Mol Genet*
244 **16**, 2272-2280, doi:10.1093/hmg/ddm179 (2007).
- 245 16 Ozata, D. M., Gainetdinov, I., Zoch, A., O'Carroll, D. & Zamore, P. D. PIWI-interacting
246 RNAs: small RNAs with big functions. *Nat Rev Genet* **20**, 89-108, doi:10.1038/s41576-
247 018-0073-3 (2019).
- 248 17 De Fazio, S. *et al.* The endonuclease activity of Mili fuels piRNA amplification that
249 silences LINE1 elements. *Nature* **480**, 259-263, doi:10.1038/nature10547 (2011).
- 250 18 Vasiliauskaitė, L. *et al.* A MILI-independent piRNA biogenesis pathway empowers
251 partial germline reprogramming. *Nat Struct Mol Biol* **24**, 604-606,
252 doi:10.1038/nsmb.3413 (2017).
- 253 19 Ariyoshi, M. & Schwabe, J. W. A conserved structural motif reveals the essential
254 transcriptional repression function of Spen proteins and their role in developmental
255 signaling. *Genes Dev* **17**, 1909-1920, doi:10.1101/gad.266203 (2003).
- 256 20 Mikami, S. *et al.* Structural insights into the recruitment of SMRT by the corepressor
257 SHARP under phosphorylative regulation. *Structure* **22**, 35-46,
258 doi:10.1016/j.str.2013.10.007 (2014).
- 259 21 Hata, K., Kusumi, M., Yokomine, T., Li, E. & Sasaki, H. Meiotic and epigenetic
260 aberrations in Dnmt3L-deficient male germ cells. *Mol Reprod Dev* **73**, 116-122,
261 doi:10.1002/mrd.20387 (2006).
- 262 22 Rogakou, E. P., Pilch, D. R., Orr, A. H., Ivanova, V. S. & Bonner, W. M. DNA double-
263 stranded breaks induce histone H2AX phosphorylation on serine 139. *J Biol Chem* **273**,
264 5858-5868 (1998).

- 265 23 Manakov, S. A. *et al.* MIWI2 and MILI Have Differential Effects on piRNA Biogenesis
266 and DNA Methylation. *Cell Rep* **12**, 1234-1243, doi:10.1016/j.celrep.2015.07.036
267 (2015).
- 268 24 Watanabe, T. *et al.* Role for piRNAs and noncoding RNA in de novo DNA methylation
269 of the imprinted mouse *Rasgrfl* locus. *Science* **332**, 848-852,
270 doi:10.1126/science.1203919 (2011).
- 271 25 Aravin, A. A. *et al.* A piRNA pathway primed by individual transposons is linked to de
272 novo DNA methylation in mice. *Mol Cell* **31**, 785-799,
273 doi:10.1016/j.molcel.2008.09.003 (2008).
- 274 26 Kloet, S. L. *et al.* Towards elucidating the stability, dynamics and architecture of the
275 nucleosome remodeling and deacetylase complex by using quantitative interaction
276 proteomics. *FEBS J* **282**, 1774-1785, doi:10.1111/febs.12972 (2015).
- 277 27 Mashtalir, N. *et al.* Modular Organization and Assembly of SWI/SNF Family
278 Chromatin Remodeling Complexes. *Cell* **175**, 1272-1288.e1220,
279 doi:10.1016/j.cell.2018.09.032 (2018).

280

281 **Supplementary Information** is linked to the online version of the paper at
282 www.nature.com/nature.

283

284 **Acknowledgements**

285 This research was supported by the Wellcome Trust funding to DOC (106144), R.B. (213612),
286 JR (103139), RCA (095021, 200885), the Wellcome Centre for Cell Biology (203149) and a
287 multi-user equipment grant (108504). DOC's laboratory is also supported by the European
288 Union H2020 program grant GermAge. A.Z. was funded by a German Research Foundation
289 fellowship (DFG, award ZO 376/1-1). We acknowledge the EMBL GeneCore facility in
290 Heidelberg, Germany for preparing the microarray dataset, RNA-seq dataset of E16.5

291 gonocytes and sequencing all next-generation sequencing libraries and namely Ferris Jung at
292 GeneCore for preparation of the Methyl-seq libraries.

293

294 **Author contributions**

295 A.Z. contributed to the design, execution and analysis of most experiments. T.A. helped
296 established the IP conditions and performed the mass-spectrometry analysis under the guidance
297 of J.R. and R.C.A. R.B. and Y.K. performed the bioinformatic analysis of the Methyl-seq data
298 or sRNA-seq as well as RNA-seq data, respectively. T.S. prepared the sRNA-seq libraries and
299 together with Y.K. the RNA-seq libraries of P20 testes. M.H and A.C. performed the homology
300 alignment of the SPOC and TFIIS-M domains. L.V. performed the IF staining of HA-MIWI2
301 and generated the gonocytes microarray dataset. Y.R.P. performed the phylogenetic analysis
302 under guidance of A.S. D.O’C. conceived and supervised this study. D.O’C. and A.Z wrote the
303 final version of the manuscript.

304

305 **Author information**

306 Reprints and permissions information is available at www.nature.com/reprints.

307 The authors declare no competing financial interests.

308 Correspondence and requests for materials should be addressed to Dónal O’Carroll

309 (donal.ocarroll@ed.ac.uk).

310

311 **Figures legends**

312

313 **Figure 1 | Definition of the MIWI2 interactome and identification of SPOCD1 from**
314 **gonocytes undergoing *de novo* genome methylation.**

315 **a**, Volcano plot showing enrichment ($\log_2(\text{mean LFQ ratio of HA-MIWI2 IP/control IP from}$
316 $\text{Miwi2}^{+/+}$ foetal testis) and confidence ($-\log_{10}(\text{P-value of two-sided Student’s t-test})$) of proteins

317 co-purifying with HA-MIWI2 from E16.5 testis lysates (n=3). Dotted line indicates factors
318 with enrichment >4-fold and significance $P < 0.05$. Red: Known piRNA pathway members,
319 blue: SPOCD1. **b**, List of known piRNA biogenesis factors and non-piRNA pathway-
320 associated proteins co-purifying with HA-MIWI2. Novel identified MIWI2 interactors are
321 underlined. **c**, Relative expression of indicated transcripts as measured by Affymetrix
322 microarray in E16.5 gonocytes (n=2), adult spermatogonia (n=3) and spermatocytes (n=3).
323 Data are mean and s.e.m., normalized to peak expression of each transcript. **d**, Schematic
324 representation of SPOCD1 domain structure.

325

326 **Figure 2 | SPOCD1 is required for spermatogenesis and LINE1/IAP silencing.**

327 **a**, Number of E16.5 embryos per plug of studs with the indicated *Spocdl* genotype mated to
328 wildtype females are presented. Data are mean and s.e.m. from n=3 *Spocdl*^{+/+} studs (9 plugs
329 total) and n=4 *Spocdl*^{-/-} studs (10 plugs total). ** $P \sim 0.001$, two-sided Student's t-test. **b**,
330 Representative images of PAS & Haematoxylin stained epididymis sections from (n=3) adult
331 mice with the indicated genotype are shown. Scale bars, 20 μm . **c**, Average testicular weight
332 in mg from adult mice with the indicated *Spocdl* genotype is plotted. Insert shows a
333 representative image of wildtype (left) and *Spocdl*^{-/-} testes. Data are mean and s.e.m. from n=3
334 wildtype and n=5 *Spocdl*^{-/-} mice. ** $P \sim 0.01$, two-sided Student's t-test. **d**, Representative PAS
335 & Haematoxylin stained testis sections of (n=3) adult mice of the indicated *Spocdl* genotype
336 is shown. Scale bars, 50 μm . **e**, **f**, Representative images of testis sections from (n=3) adult
337 wildtype and *Spocdl*^{-/-} mice stained for LINE1 ORF1p (**e**) or IAP-GAG protein (**f**) (red) are
338 shown. DNA was stained with DAPI (blue). Scale bars, 50 μm . **g**, RNA-seq derived heat maps
339 depicting fold-change of expression relative to wildtype for the 10 most up-regulated LINE
340 and ERVK TEs in (n=3) *Miwi2*^{-/-} and *Spocdl*^{-/-} P20 testis. **h**, **i**, Representative images of testis
341 sections of (n=3) adult wildtype and *Spocdl*^{-/-} mice stained for the DNA damage response

342 marker γ H2AX (h) and TUNEL staining revealing apoptotic cells (i) (red). DNA was stained
343 with DAPI (blue). Scale bars, 50 μ m.

344

345 **Figure 3 | SPOCD1 is required for *de novo* TE DNA methylation loci but not piRNA**
346 **expression.**

347 **a-e**, Analyses of genomic CpG methylation of undifferentiated P14 spermatogonia from (n=3)
348 wildtype, *Spocd1*^{-/-} and *Miwi2*^{-/-} mice are presented. **a, b**, Percentages of CpG methylation
349 levels of the indicated genomic features (with genic, promoter and CpG islands non-
350 overlapping TEs and intergenic non-overlapping TEs or genes) or TEs (non-overlapping genes)
351 for (n=3) biological replicates per genotype is shown as box plots. Boxes represent
352 interquartile range from 25th to 75th percentile, the horizontal line the median, whiskers denote
353 the data range of median \pm 2x interquartile range and dots datapoints outside of this data range.
354 **c**, Metaplots of mean CpG methylation over LINE1 elements and adjacent 2 kb are shown. **d**,
355 Correlation analysis of mean CpG methylation loss relative to wildtype for individual TEs of
356 the indicated LINE1 family in relation to their divergence from the consensus sequence is
357 shown for *Spocd1*^{-/-} spermatogonia. **e**, Heatmap of mean CpG methylation level of indicated
358 maternal and paternal imprinted regions is shown. *Rasgrfl* imprinted control region is shown
359 in detail. **f-h**, piRNA analysis of small RNAs sequenced from E16.5 testes from (n=3)
360 *Spocd1*^{+/-} and *Spocd1*^{-/-} mice is presented. **f**, Nucleotide (nt) length distribution of small RNAs
361 is shown. Data represent the mean and s.e.m. No significant differences were observed (P=1.0,
362 Bonferroni adjusted two-tailed Student's t-tests). **g**, Annotation of piRNAs from merged
363 replicates. **h**, Ping-pong analysis of piRNAs: Relative frequency of the distance between 5'
364 ends of complementary piRNAs mapping to the LINE1 L1Md_T family is shown. **i**,
365 Representative images (of n=3 wildtype and *Spocd1*^{-/-} mice) of MIWI2 localization in E16.5

366 *Spocd1*^{+/-} and *Spocd1*^{-/-} gonocytes. Scale bars, 15 μ m. Insert shows a zoom in of the indicated
367 cell. Scale bars, 2 μ m.

368

369 **Figure 4 | SPOCD1 is a nuclear protein that associates with the *de novo* DNA methylation**
370 **machinery and repressive chromatin remodelling complexes.**

371 **a**, Schematic representation of the *Spocd1*^{HA} allele and the C-terminal HA-tagged SPOCD1
372 protein. **b**, Representative image of SPOCD1-HA localization in gonocytes at E16.5 from
373 (n=3) *Spocd1*^{HA/+} mice. Scale bar, 20 μ m. Insert shows a zoom in of the indicated foetal
374 gonocyte. Scale bar, 2 μ m. **c, d**, Representative images of expression of SPOCD1-HA (c) and
375 HA-MIWI2 (d) in gonocytes at the indicated time points from (n=3) *Spocd1*^{HA/+} and *Miwi2*
376 ^{HA/+} mice, respectively, are shown. Scale bars, 2 μ m. **e**, Volcano plot showing enrichment
377 (\log_2 (mean LFQ ratio of SPOCD1-HA IP/control IP from *Spocd1*^{+/+} foetal testis) and statistical
378 confidence ($-\log_{10}$ (P-value of two-sided Student's t-test)) of proteins co-purifying with
379 SPOCD1-HA from E16.5 testis lysates (n=4). Dotted line indicates enrichment >4-fold and
380 significance P<0.05. DNMT3L and DNMT3A (green), members of the NURD (violet) and
381 BAF (blue) complexes are highlighted. **f**, Schematic representation of selected proteins co-
382 purifying with SPOCD1. **g**, Volcano plot as presented in panel e of proteins co-purifying with
383 MIWI2-HA from E16.5 testis Benzonase-solubilized extracts (n=4). **h**, Schematic
384 representation of overlap of proteins co-purifying with both SPOCD1 and MIWI2.

385

386 **Methods**

387

388 **Mouse strains and experimentation**

389 The *Miwi2*^{HA} and *Miwi2*^{tdTomato} (*Miwi2*^{tdTom}) mouse alleles have been previously produced in
390 the O'Carroll laboratory^{18,28}. These lines were kept on a C57BL/6N genetic background. The

391 *Miwi2^{tdTom}* mouse allele generates a null allele and was used as a *Miwi2^{null}* allele in this study²⁸.
392 The *Spocd1^{null}* and *Spocd1^{HA}* alleles were created using CRISPR-Cas9 gene editing technology
393 using B6CBAF1/Crl genetic background fertilized 1-cell zygotes as previously described^{29,30}.
394 For *Spocd1^{null}*, we injected a single sgRNA (GCAGGTTGAAGAGCAGGCTG) together with
395 CAS9 mRNA and F₀ offspring screened by PCR and Sanger sequencing for frame-shift
396 mutations. The *Spocd1^{HA}* allele was generated by injection of a single sgRNA
397 (CCCCTCCTCAGATTCAGCAT) together with CAS9 mRNA and a single stranded DNA
398 oligo containing a GGGGS linker, HA-epitope tag and a PAM site mutation flanked by 72
399 nucleotides of homology arms
400 (AAACAGACTGCAGAACAGATACAACTAGGCAGGTGTGGGAGAGCTCACTCGC
401 CCCTCCTCAGATTCAGCATcGTAAAGGAATCAAGCGTAATCTGGAACATCGTAT
402 GGGTAGGATCCTCCGCCTCCACACTCATGTTCTGGTGGCTCTAAAGGGTCTGACC
403 CCTCTGGTGGGGGACAGTTAGAGCCACCTCCATCCA). F₀ offspring were then
404 screened by PCR and Sanger sequencing for the correct allele. Both lines were established from
405 one founder animal and back-crossed several times to a C57BL/6N genetic background. Thus,
406 the mice analysed were on a mixed B6CBAF1/Crl; C57BL/6N genetic background. Mice were
407 genotyped by PCR using the following primer pairs, *Spocd1^{null}* (F:
408 GAAGATGAGGTAGAGGCCATCG, R: TGAGCCACTTTGAGAAACAGGT) and
409 *Spocd1^{HA}* (F: CCCCATCCACTGTAGTATCTGC, R: ATACAACTAGGCAGGTGTGGG).
410 For foetal testes collection for IP-MS, the *Miwi2^{HA}* line was additionally back-crossed twice to
411 an Hsd:ICR (CD1) outbred genetic background, which shows a characteristic large litter size
412 (*Miwi2^{HA}*.CD1). Mice were mated for 4 days and females checked for plugs daily. Plugged
413 females were separated from studs and the day of the plug counted as E0.5. Foetal testes for
414 the immuno-precipitation and mass-spectrometry experiments were collected from matings of
415 *Miwi2^{HA/HA}* studs to *Miwi2^{HA/HA}* females or *Spocd1^{HA/HA}* studs to Hsd:ICR (CD1) wildtype

416 females. Male fertility was assessed by mating studs to Hsd:ICR (CD1) wildtype females
417 counting the number of embryos at E16.5 for each plugged female. Female fertility was
418 assessed by mating *Spocd1*^{-/-} females to *Spocd1*^{+/-} studs and comparing number of embryos at
419 E16.5 for each plugged female to matings of C57BL/6N wildtype mice.

420 Animals were maintained at the University of Edinburgh, UK in accordance with the regulation
421 of the UK Home Office. Ethical approval for the mouse experimentation has been given by the
422 University of Edinburgh's Animal Welfare and Ethical Review Body and the work done under
423 licence from the United Kingdom's Home Office.

424

425 **Immuno-precipitation and mass-spectrometry (IP-MS)**

426 Foetal testes were isolated from E16.5 embryos and snap frozen in liquid nitrogen. 50 testes
427 per replicate were lysed and homogenized in 1 ml of hypotonic lysis buffer (10 mM Tris-HCl
428 pH 8, 10 mM KCl, 5 mM MgCl₂, 0.1 % IGEPAL CA-630, complete protease inhibitor EDTA-
429 free (Roche)) with 20 strokes in a glass douncer. For the IP-MS experiments presented in figure
430 4, lysates of *Spocd1*^{HA/+} or *Miwi2*^{HA/+} testes and corresponding wildtype controls were further
431 incubated for 30 min at 4 °C after addition of 50 U/ml Benzonase (Millipore). Lysates were
432 cleared by centrifugation for 10 min at 21,000 x g. 50 µl anti-HA magnetic beads (Pierce)
433 (additionally cross-linked with 20 mM dimethyl-pimelidate in borate buffer pH 9) were
434 resuspended in 600 µl hypotonic lysis buffer. 900 µl of cleared lysate was then added to the
435 resuspended beads and incubated for 30 min at 4 °C. Beads were washed four times with wash
436 buffer (50 mM Tris-HCl pH 8, 100 mM KCl, 5 mM MgCl₂, 0.1 % IGEPAL CA-630) and
437 bound proteins were eluted with 0.1 % Rapigest (Waters) in 50 mM Tris-HCl pH 8 for 15 min
438 at 50 °C.

439 Eluted proteins were trypsin digested as described³¹, desalted using STAGE tips³², resuspended
440 in 0.1 % trifluoroacetic acid (v/v) and subjected to LC-MS. Peptides were separated on an ultra-

441 high resolution nano-flow liquid chromatography nanoLC Ultimate 3000 unit fitted with an
442 Easyspray (50 cm, 2 μ m particles) column coupled to the high resolution/accurate-mass mass-
443 spectrometer Orbitrap Fusion Lumos operated in DDA(data-dependent-acquisition)-mode
444 (Thermo Fisher Scientific). Samples we separated using a 2 % - 40 % - 95 % 190 min gradient
445 (Mobile phase A - 0.1 % aqueous formic acid, B – 80 % acetonitrile in 0.1 % formic acid). The
446 MS acquisition parameters were as follows – cycle time was set to 3 s, the MS1 scan Orbitrap
447 resolution was set to 120,000, RF lens to 30 %, AGC target to 4.0e5, and maximum injection
448 time to 50 ms, detected intensity threshold was 5.0e3. The MS2 scan was performed with the
449 Ion Trap using rapid scan setting. The AGC target was set to 2.0e4, and maximum injection
450 time was 50ms. This set-up achieves a detection limit in the low attomole (10^{-18})-range and has
451 been used in large proteome and interactome screens^{33,34}. Raw data were processed using
452 MaxQuant version 1.6.1.0. Label-free quantitation (LFQ) was performed using the MaxQuant
453 LFQ algorithm³⁵. Peptides were searched against the mouse UniProt database (date
454 21.07.2017) with commonly observed contaminants (e.g. trypsin, keratins, etc.) removed
455 during Perseus analysis³⁵⁻³⁷. For visualization, LFQ intensities were imported into Perseus
456 version 1.6.0.2³⁷ and processed as described³⁸.

457

458 **Nuclear localization signal (NLS) prediction**

459 The presence of an NLS was predicted by cNLS mapper³⁹, searching the entire protein for
460 bipartite NLSs and a cut-off score of 5.0.

461

462 **Affymetrix microarray datasets**

463 The Affymetrix microarray datasets of spermatogonia, spermatocytes, mouse embryonic
464 fibroblasts (MEFs) and bone marrow (ArrayExpress: E-MTAB-4828, E-MTAB-7067, E-
465 MTAB-5056) have been previously described^{28,40,41}. The new microarray data for gonocytes

466 was generated as previously described⁴⁰ from gonocytes purified by FACS from E16.5 foetal
467 testes using the *Miwi2^{tdTom}* reporter allele²⁸.

468

469 **Domain alignment**

470 Alignments of SPOCD1 domains to homologous proteins were generated using ClustalW⁴².

471 Alignment of the SPOC domain was adjusted based on SPOCD1 models generated by

472 PHYRE2⁴³ superimposed on human SHARP (PDBid 1OW1¹⁹) and *A. thaliana* FPA SPOC

473 (PDBid 5KXF⁴⁴) domains. Alignments are presented using Jalview⁴⁵ with secondary structure

474 elements from human SHARP (PDBid 1OW1¹⁹), PHF3 (PDBid 2DME) and human TFIIS

475 (PDBid 3NDQ). The following sequence identifiers of homologues were used in the alignment

476 of the SPOCD1 SPOC domain: Q6ZMY3, H9GUJ8, F7FFW6, B2RQG2, Q92576, H9GF02,

477 B8A483, XP_028916420.1, Q8C9B9, Q9BTC0, G1KE55, F1QQA3, F7DIQ2, Q62504,

478 Q96T58, H9GKA7, F1QMN6, XP_028921280.1. The SPOCD1 TFIIS-M domain was aligned

479 based on primary sequence to the following sequences: Q6ZMY3, H9GUJ8, F7FFW6,

480 B2RQG2, Q92576, H9GF02, B8A483, XP_028916420.1, Q8C9B9, Q9BTC0, G1KE55,

481 F1QQA3, F7DIQ2, P10711, P23193, H9GPX5, Q7T3C1, F7BX76.

482

483 **Phylogenetic analyses**

484 *Spocd1*, *Phf3* and *Didol* sequences were searched via tblastn⁴⁶ using the mouse and alligator

485 protein sequences as queries and the non-redundant nucleotide collection as database.

486 Transcript sequences with significant alignments were downloaded and processed to keep only

487 cDNA sequences. Additional cDNA sequences were included based on described orthologous

488 relationships from Ensembl 90⁴⁷ and Ensembl 91⁴⁸. Axolotl and western clawed frog sequences

489 were extracted from the UCSC genome browser⁴⁹. *Didol* orthologous sequences from

490 *Drosophila* and *C. elegans* were identified by the ortholog annotations of Flybase⁵⁰ (release

491 FB2017_05). For phylogeny reconstruction including only *Spocd1* orthologs, cDNA sequences

492 were aligned using the RevTrans 2.0b webserver⁵¹ with T-COFFEE (v.11.0) as alignment
493 method. For the phylogeny including *Spocd1* and its paralogs, cDNA sequences were first
494 virtually translated with the Virtual Ribosome tool version 2.0⁵² and aligned using Clustal
495 Omega^{42,53} with default parameters. Protein alignments were saved and used as scaffolds to
496 align cDNA sequences using the RevTrans 2.0b webserver. Nucleotide alignments generated
497 by RevTrans were formatted into NEXUS interleave files that were used for phylogenetic
498 reconstruction with MrBayes v3.2.6^{54,55} through the CIPRES Science Gateway V. 3.3⁵⁶. The
499 selected evolutionary model for MrBayes was *GTR + I + Γ* (nst=6 rates=invgamma) and priors
500 on state frequencies were left with default values. Two analyses (nruns=2) were run with four
501 MCMC chains for each one (nchains=4) and a heating parameter of 0.2. Sample and diagnostic
502 frequencies were set to 1,000 and 5,000, respectively. Analyses were stopped after 2×10^6
503 generations and the consensus trees were obtained using a burnin fraction of 0.25. Tree
504 appearance was edited with FigTree v1.4.2 (<http://tree.bio.ed.ac.uk/software/figtree>).

505

506 **Histology**

507 Isolated testes and epididymis were fixed overnight in Bouin's fluid, washed three times in 70
508 % ethanol and embedded in paraffin. 6 μ m sections were cut on a microtome (Leica) and
509 deparaffinised in a graded alcohol series according to standard laboratory procedures. The
510 rehydrated sections were then stained with the periodic-acid-Schiff (PAS) staining kit (TCS
511 Biosciences) according to the manufacturer's recommendations. The stained sections were
512 subsequently de-hydrated in a reverse alcohol series and mounted on coverslips with Pertex
513 mounting media (Pioneer Research Chemicals) according to standard laboratory procedures.
514 Slides were imaged on a Zeiss AxioScan scanning microscope using the 40x objective.
515 Cropped images of the scan were exported using the Zeiss Zen software and further processed
516 in ImageJ.

517

518 **Immuno-fluorescence**

519 Immuno-fluorescence was performed on freshly cut 6 μm sections of OCT embedded testes as
520 previously described¹⁸ Primary antibodies were incubated overnight in blocking buffer
521 (dilutions: anti-HA (C29F4, Cell Signaling Technologies) 1:200 (for SPOCD1-HA) or 1:500
522 (for HA-MIWI2); anti-HA (6E2, Cell Signaling Technologies) 1:200; anti-LINE1-ORF1P⁵⁷
523 1:500; anti-IAP-GAG (a kind gift from B. Cullen, Duke University, Durham, NC, USA) 1:500;
524 anti- γ H2AX (IHC-00059, Bethyl Laboratories) 1:500), anti-SCP1 (ab15090, abcam) 1:300 and
525 anti-SCP3 (D1, sc74569, Santa Cruz Biotechnology) 1:300. Sections were then stained with
526 DAPI and the appropriate donkey anti-rabbit or donkey anti-mouse labelled with an Alexa
527 Fluor (488, 568 or 647) dye and mounted on coverslips with Prolong Gold (Invitrogen). Images
528 were acquired on a Zeiss Observer, Leica SP8 confocal microscope or Zeiss LSM880 with
529 Airyscan module. Images acquired using the Airy scan module were deconvoluted with the
530 Zeiss Zen software “Airyscan processing” on settings “3D” and a strength of 6. Images were
531 processed and analysed with ImageJ and Zeiss Zen software.

532

533 **Terminal deoxynucleotidyl transferase dUTP nick end labelling (TUNEL assay)**

534 Paraffin embedded testes were sectioned and re-hydrated as described above. Sections were
535 pre-treated with proteinase K (10 $\mu\text{g}/\text{ml}$ in 10 mM Tris pH 8; Thermo Scientific) and labelled
536 using the Click-iT TUNEL assay, Alexa Fluor 647 dye (Invitrogen) according to the
537 manufacturer’s instructions. Sections were counter-stained with DAPI (1 $\mu\text{g}/\text{ml}$), embedded
538 with Prolong Gold (Invitrogen) and imaged on a Zeiss Observer microscope. Images were
539 processed as above.

540

541 **RNA sequencing and analysis**

542 Total RNA was extracted from sorted *Miwil2^{tdTOM}*-positive E16.5 gonocytes using QIAzol
543 reagent (Qiagen). Libraries for low input RNA-seq were then prepared with RiboGone and the
544 SMARTer Stranded RNA-seq kit from Clontech and sequenced on an Illumina HiSeq 4000 in
545 75 bp paired-end mode. For RNA-seq of P20 testis, total RNA was extracted from 1 testis using
546 QIAGEN RNeasy Mini kit, following the manufacturer's protocol including on-column DNase
547 treatment. Total RNA was used for library preparation with NEBNext Ultra II Directional RNA
548 Library Prep Kit for Illumina and 8 cycles of PCR was performed. These libraries were
549 sequenced on an Illumina NextSeq 500 in 150 bp single-end read mode.
550 For analysis of differentially expressed genes, reads were mapped to GRCm38 genome_tran
551 (release 84) with HISAT2(2.1.0)⁵⁸ using following options: --no-mixed --no-discordant --qc-
552 filter --trim5 3. Mapped reads per gene were counted with htseq-count (HTSeq 0.11.1)⁵⁹
553 providing a GTF file and differentially expressed genes were analysed using DESeq2(1.26.0)⁶⁰.
554 For analysis of differentially expressed retrotransposons, adapter sequences were removed
555 from reads using cutadapt(1.8.1)⁶¹ with default settings. Processed reads were mapped to
556 consensus sequence of rodent retrotransposons retrieved from Repbase(24.01)⁶² using
557 bowtie2⁶³ (2.3.4.3) with default settings. Mapped reads per retrotransposon were counted and
558 significantly de-regulated species were analysed using DESeq2.

559

560 **Fluorescence activated cell sorting (FACS)**

561 CD9⁺ spermatogonia were sorted from P14 testes as previously described¹⁸ with minor
562 alterations: 100 µg/ml DNase I (Sigma-Aldrich) was added together with foetal calf serum to
563 stop the trypsin digest and the cell suspension was further incubated for 3 min at 32 °C to
564 facilitate complete degradation of released DNA. Cells were blocked with Fc block (anti-
565 CD16/32, clone 93, eBioscience, 1:50), followed by labelling with anti-CD45 (clone 30-F11,
566 eBioscience, 1:200) and anti-CD51 (clone RMV-7, Biolegend, 1:50) biotin conjugated

567 antibodies. Cells were then stained with anti-CD9^{APC} (clone eBioKMC8, eBioscience, 1:200),
568 anti-cKit^{PE-Cy7} (clone 2B8, eBioscience, 1:1600), streptavidin^{V450} (BD bioscience, 1:250) and
569 1 µg/ml DAPI and sorted into medium on a BD Aria II sorter (gating strategy shown in
570 Supplementary Figure 2a). Sorted cells were pelleted for 5 min at 500 g and snap frozen in
571 liquid nitrogen.

572 E16.5 gonocytes were FACS purified from *Miw12^{tdTom/+}* foetal testes by dissecting the testes in
573 a drop of goni-mem (DMEM (Life Technologies) supplemented with penicillin-streptomycin
574 (Life Technologies), NEAA (Life Technologies), sodium pyruvate (Life Technologies) and
575 sodium lactate (Sigma-Aldrich) and digestion in 0.25 % Trypsin-EDTA (Gibco) at 37 °C for
576 10 minutes. Digestion was stopped by addition of 20 % foetal calf serum (FCS) and cells
577 pelleted for 5 min at 100 x g. The pellet was treated with 10 µl 5 mg/ml DNase I (Sigma-
578 Aldrich) for 2 min and cells rigorously resuspended in PBS containing 2 % FCS by pipetting
579 50 times. tdTomato-positive cells were sorted on a BD Aria Fusion sorter into PBS, lysed in
580 Qiazol (Qiagen) and snap frozen in liquid nitrogen (gating strategy shown in Supplementary
581 Figure 2b).

582

583 **Whole genome methylation sequencing (Methyl-seq) and analysis**

584 DNA from FACS-isolated P14 spermatogonial stem cells was isolated by proteinase K digest
585 (10 mM Tris-HCl pH 8 , 5 mM EDTA , 1 % SDS, 0.3 M Na-acetate, 0.2 mg/ml proteinase K)
586 overnight, followed by two rounds of phenol/chloroform/isoamylalcohol (25:24:1, Sigma-
587 Aldrich) extraction and one round of chloroform extraction. The DNA was precipitated at -20
588 °C after addition of 1/10 volume 3 M Na-acetate, 10 µg linear acrylamide (Invitrogen) and 1
589 volume of isopropanol, washed two times and solubilized in 5 mM Tris-HCl pH 8. Methyl-seq
590 libraries were prepared using the NEBnext Enzymatic Methyl-seq kit (NEB) according to the
591 manufacturer's instructions and sequenced by Illumina NextSeq and HiSeq sequencing in 150

592 bp paired-end read mode. Whole genome bisulfite sequencing (WGBS) datasets of adult *Mili-*
593 *-* spermatocytes⁴ and P10 *Dnmt3c^{+/-}, Dnmt3c^{-/-}, Dnmt3l^{+/-}, Dnmt3l^{-/-}* germ cells¹² were obtained
594 from public repositories (accession numbers SRP037785 and GSE84140, respectively).

595 Raw sequence reads were trimmed to remove both poor-quality calls and adapters using Trim
596 Galore (v0.4.1, www.bioinformatics.babraham.ac.uk/projects/trim_galore/, Cutadapt⁶¹ version
597 1.8.1, parameters: `--paired --length 25 --trim-n --clip_R2 5`). Trimmed reads were aligned to
598 the mouse genome in paired-end mode to be able to use overlapping parts of the reads only
599 once. Alignments were carried out with Bismark v0.22.1⁶⁴ with the following set of parameters:
600 `bismark --score_min L,0,-0.4 --paired`. CpG methylation calls were extracted from the
601 deduplicated mapping output using the Bismark methylation extractor (v0.22.1). The mapping
602 statistics were calculated using the SeqMonk
603 (www.bioinformatics.babraham.ac.uk/projects/seqmonk/) datastore summary report of aligned
604 deduplicated bam files. The methylation conversion rate was calculated by mapping all reads
605 to the spiked-in CpG unmethylated lambda and CpG methylated pUC19 DNA using the
606 Bismark pipeline as outlined above (Supplementary Table 7).

607 50 adjacent CpG running window probes were generated for probes containing at least 10 reads
608 and mean percentage methylation of the 3 replicates was calculated for each probe. For analysis
609 of specific genome features these were defined as follows: Genic regions were defined as
610 probes overlapping genes and promoter as probes overlapping 2000 bp upstream of annotated
611 transcripts, as annotated by Ensembl (GRCm38.p6). CpG islands (CGIs) probes overlapping
612 the Ensembl (GRCm38.p6) CGI annotation. For genic, promoters and CGIs genome features
613 reads overlapping transposons were filtered out. For transposons, UCSC repeat masker
614 annotations were downloaded from the table browser ([https://genome.ucsc.edu/cgi-](https://genome.ucsc.edu/cgi-bin/hgTables)
615 `bin/hgTables`, 02/2019). The transposon annotation, which includes retro- and DNA
616 transposons, was sorted to exclude simple repeats as well as any small non-coding RNA

617 annotations. Analysis of TEs in our data was performed by unique mapping in the genome and
618 excluding any repeats overlapping gene bodies. Transposon families were assessed by mapping
619 only to full length elements defined as > 5 kb for LINE1 elements, > 6 kb for IAP families and
620 > 4.5 kb for MMERVK10C. Intergenic regions were defined as regions non-overlapping genes
621 or transposons. The methylation level was expressed as the mean percentage of individual CG
622 sites. The metaplots, scatterplots and correlation analysis were performed by extracting the
623 reads overlapping the respective genomic regions from SeqMonk and plotting in RStudio. The
624 methylation difference analysis was performed using the divergence (milliDiv) from the
625 consensus sequences. We extracted the imprinted control regions (ICR) from
626 (<https://atlas.genetics.kcl.ac.uk/>). For CpG methylation of the *Rasgrfl* imprinted region we
627 quantified individual CpGs with a minimum of 1 read mapping. Graphing and statistics were
628 performed using SeqMonk and RStudio.

629

630 **Small RNA sequencing (sRNA-seq) and analysis**

631 For each replicate, 6 foetal testes were pooled and RNA was isolated using the QIAzol reagent
632 following the manufacturer's instructions. Total RNA was size selected for 15–40 nucleotides
633 (nt) using a 15 % TBE-Urea gel (Invitrogen) and a small RNA marker (Abnova) with 2x Gel
634 loading Buffer II (Ambion). RNA was purified from the gel by addition of nuclease-free water
635 and two successive 1 hour incubation steps at 37 °C, 1000 rpm with a freeze/thaw step in
636 between. Samples were then transferred onto spin columns (Corning) plugged with filter paper
637 (Whatman) and centrifuged at max speed for 1 min. RNA was precipitated overnight at -20 °C
638 in 2.5 volumes ethanol 100 % and 1 µl GlycoBlue (Life Technologies), washed with 80 %
639 ethanol and dissolved in 10 µl nuclease-free water. For generation of the library the NEBnext
640 Multiplex Small RNA Library Prep Set for Illumina (NEB) was used following the
641 manufacturer's instructions with 4 µl size-selected RNA per reaction, adaptors diluted 1:2 and

642 16 cycles of PCR amplification. Concentration was measured with the Qubit high sensitivity
643 dsDNA kit on a Qubit fluorometer (Life Technologies) and quality of the library was checked
644 using a HSD1000 tape on a TapeStation 2200 instrument (Agilent). 4 ng of each sample were
645 used for the final library pool and sequenced on a HiSeq2500 sequencer (Illumina) in 50 bases
646 single-end read mode.

647 Adapter sequences were removed from 3' end of the raw fastq file using cutadapt⁶¹ with default
648 settings. Annotation of processed reads of 18–32 nt for each sample were retrieved as
649 described⁶⁵ using bowtie 1.2.1.1⁶⁶. Up to 3 mismatches were allowed when reads were mapped
650 to genomic TE sequences retrieved from RepeatMasker(mm10, October 2015). Mapped
651 piRNA reads (25–30 nt) were categorized according to annotations with reads not mapping to
652 any recorded genomic element included in 'other'. To compare expression of individual
653 piRNAs, only mapped reads of 25–30 nt with more than 10 counts were considered and
654 visualised as scatter plot. The piRNA amplification analysis and mapping of LINE1 and IAP
655 was performed as described¹⁷. The consensus sequence of L1MdTfI, L1MdGfI, IAPEYI and
656 IAPEZI were retrieved from Repbase⁶².

657

658 **Cell culture, transfection and IP-Western blot**

659 HEK 293T cells (sourced from the O'Carroll laboratory stock, University of Edinburgh; not
660 additionally authenticated and regularly tested for mycoplasma contamination) were cultured
661 at 37 °C, 5 % CO₂ in Glasgow minimum essential medium (Sigma Aldrich) supplemented with
662 10 % foetal calf serum (Gibco), 2 mM L-glutamine and 1 mM Na-pyruvate (Invitrogen). For
663 transfection 4*10⁵ cells were seeded per well on a 6-well plate on day 0 followed by
664 transfection of 1 µg of each plasmid (pcDNA3.1-DNMT3A-FLAG: GenScript clone ID
665 OMu22132D; pcDNA3.1-DNMT3L-FLAG: GenScript clone ID OMu18257D; pcDNA3.1-
666 DNMT3C-FLAG: encoding the long isoform as defined by Barau et al. 2016¹², synthesised by

667 GenScript; pcDNA3.1-SPOCD1-HA: encoding XP_017175994.1, synthesised by GenScript)
668 by Jetprime transfection (Polyplus) according to the manufacturer's instructions on day 1. 65
669 hours later cells were washed twice with ice-cold PBS, scrapped of the plate in 1 ml lysis buffer
670 (IP buffer: 150 mM KCl, 2.5 mM MgCl₂, 0.5 % Triton X-100, 50 mM Tris pH 8, supplemented
671 with 1x protease inhibitors (cOmplete ULTRA EDTA-free, Roche) and 37 U/ml Benzonase
672 (Millipore)) and lysed for 30 minutes at 4 °C on a rotating wheel. Lysates were cleared for 5
673 minutes at 21,000 g and 400 µl each was incubated for 2 hours at 4 °C with 20 µl of anti-HA
674 beads (Pierce) and 20 µl control Protein G Dynabeads (Life Technologies), which had been
675 washed twice in PBS, 0.5 % Triton X-100 and resuspended in 500 µl lysis buffer. Immuno-
676 precipitates were eluted for 10 minutes at 50 °C in 35 µl 0.1 % SDS (sodium dodecyl sulfate),
677 50 mM Tris pH 8. Lysates and eluates were separated on a 4-12 % bis-tris acrylamide gel
678 (Invitrogen) and blotted onto nitrocellulose membrane (Amersham Protran 0.45 NC) according
679 to standard laboratory procedures. The membrane was stained for protein with 0.1 % (w/v)
680 Ponceau S in 5 % (v/v) acetic acid solution for 5 minutes, blocked with blocking buffer (4 %
681 (w/v) skimmed milk powder (Sigma-Aldrich) in TBS-T (tris buffered saline, 0.1 % Tween-
682 20)), incubated with primary antibodies for 1 hour (anti-HA (6E2, Cell Signaling
683 Technologies) 1:1000; anti-FLAG (M2, Sigma-Aldrich) 1:1000) in blocking buffer, washed 4
684 times for 5 minutes in TBS-T, incubated with secondary antibodies (IRDye 680RD donkey
685 anti-rabbit & IRDye 800CW donkey anti-mouse, LI-COR, 1:10,000) in Immobilon® Block –
686 PO blocking solution (Millipore), washed 4 times for 5 minutes in TBS-T and imaged on a LI-
687 COR Odyssey Fc system. Exposure of the entire images was adjusted in Image Studio Lite (LI-
688 COR) and regions of interest cropped for presentation.

689

690 **Statistical information**

691 Statistical testing was performed with R(3.3.1) using the R Studio software and with Perseus
692 for the mass-spectrometry data. Unpaired, two-tailed Student's t-tests were used to compare
693 differences between groups and adjusted for multiple testing using Bonferroni correction where
694 indicated, except for RNA-seq data analysis where Wald's tests and Benjamini-Hochberg
695 correction were used. Averaged data are presented as mean \pm s.e.m. (standard error of the
696 mean), unless otherwise indicated. No statistical methods were used to predetermine sample
697 size. The experiments were not randomized and the investigators were not blinded to allocation
698 during experiments and outcome assessment.

699

700 **Data availability**

701 All mRNA expression data that support the findings of this study have been deposited at Array
702 Express under accession numbers E-MTAB-7985. The Methyl-seq data generated in this study
703 have been deposited at ArrayExpress under the accession number E-MTAB-7997. The sRNA-
704 seq and RNA-seq data generated in this study have been deposited at Gene Expression
705 Omnibus under the accession number GSE131377. Data for the IP-MS experiments were
706 deposited at ProteomeXchange under the accession number PXD016701.

707

708 **Code availability**

709 Scripts used for the Methyl-seq, RNA-seq and sRNA-seq analysis are available on github
710 (https://github.com/rberrens/SPOCD1-piRNA_directed_DNA_met).

711

712 **Additional References**

713

714 28 Carrieri, C. *et al.* A transit-amplifying population underpins the efficient regenerative
715 capacity of the testis. *J Exp Med* **214**, 1631-1641, doi:10.1084/jem.20161371 (2017).

- 716 29 Wang, H. *et al.* One-step generation of mice carrying mutations in multiple genes by
717 CRISPR/Cas-mediated genome engineering. *Cell* **153**, 910-918,
718 doi:10.1016/j.cell.2013.04.025 (2013).
- 719 30 Yang, H. *et al.* One-step generation of mice carrying reporter and conditional alleles by
720 CRISPR/Cas-mediated genome engineering. *Cell* **154**, 1370-1379,
721 doi:10.1016/j.cell.2013.08.022 (2013).
- 722 31 Wiśniewski, J. R., Zougman, A., Nagaraj, N. & Mann, M. Universal sample preparation
723 method for proteome analysis. *Nat Methods* **6**, 359-362, doi:10.1038/nmeth.1322
724 (2009).
- 725 32 Rappsilber, J., Ishihama, Y. & Mann, M. Stop and go extraction tips for matrix-assisted
726 laser desorption/ionization, nanoelectrospray, and LC/MS sample pretreatment in
727 proteomics. *Anal Chem* **75**, 663-670 (2003).
- 728 33 Hein, M. Y. *et al.* A human interactome in three quantitative dimensions organized by
729 stoichiometries and abundances. *Cell* **163**, 712-723, doi:10.1016/j.cell.2015.09.053
730 (2015).
- 731 34 Richards, A. L. *et al.* One-hour proteome analysis in yeast. *Nat Protoc* **10**, 701-714,
732 doi:10.1038/nprot.2015.040 (2015).
- 733 35 Cox, J. *et al.* Accurate proteome-wide label-free quantification by delayed
734 normalization and maximal peptide ratio extraction, termed MaxLFQ. *Mol Cell*
735 *Proteomics* **13**, 2513-2526, doi:10.1074/mcp.M113.031591 (2014).
- 736 36 The UniProt Consortium. UniProt: the universal protein knowledgebase. *Nucleic Acids*
737 *Res* **45**, D158-D169, doi:10.1093/nar/gkw1099 (2017).
- 738 37 Tyanova, S. *et al.* The Perseus computational platform for comprehensive analysis of
739 (prote)omics data. *Nat Methods* **13**, 731-740, doi:10.1038/nmeth.3901 (2016).

- 740 38 Hubner, N. C. & Mann, M. Extracting gene function from protein-protein interactions
741 using Quantitative BAC InteraCtomics (QUBIC). *Methods* **53**, 453-459,
742 doi:10.1016/j.ymeth.2010.12.016 (2011).
- 743 39 Kosugi, S., Hasebe, M., Tomita, M. & Yanagawa, H. Systematic identification of cell
744 cycle-dependent yeast nucleocytoplasmic shuttling proteins by prediction of composite
745 motifs. *Proc Natl Acad Sci U S A* **106**, 10171-10176, doi:10.1073/pnas.0900604106
746 (2009).
- 747 40 Morgan, M. *et al.* mRNA 3' uridylation and poly(A) tail length sculpt the mammalian
748 maternal transcriptome. *Nature* **548**, 347-351, doi:10.1038/nature23318 (2017).
- 749 41 Morgan, M. *et al.* A programmed wave of uridylation-primed mRNA degradation is
750 essential for meiotic progression and mammalian spermatogenesis. *Cell Res* **29**, 221-
751 232, doi:10.1038/s41422-018-0128-1 (2019).
- 752 42 Sievers, F. *et al.* Fast, scalable generation of high-quality protein multiple sequence
753 alignments using Clustal Omega. *Mol Syst Biol* **7**, 539, doi:10.1038/msb.2011.75
754 (2011).
- 755 43 Kelley, L. A., Mezulis, S., Yates, C. M., Wass, M. N. & Sternberg, M. J. The Phyre2
756 web portal for protein modeling, prediction and analysis. *Nat Protoc* **10**, 845-858,
757 doi:10.1038/nprot.2015.053 (2015).
- 758 44 Zhang, Y., Rataj, K., Simpson, G. G. & Tong, L. Crystal Structure of the SPOC Domain
759 of the Arabidopsis Flowering Regulator FPA. *PLoS One* **11**, e0160694,
760 doi:10.1371/journal.pone.0160694 (2016).
- 761 45 Waterhouse, A. M., Procter, J. B., Martin, D. M., Clamp, M. & Barton, G. J. Jalview
762 Version 2--a multiple sequence alignment editor and analysis workbench.
763 *Bioinformatics* **25**, 1189-1191, doi:10.1093/bioinformatics/btp033 (2009).

764 46 Altschul, S. F. *et al.* Gapped BLAST and PSI-BLAST: a new generation of protein
765 database search programs. *Nucleic Acids Res* **25**, 3389-3402,
766 doi:10.1093/nar/25.17.3389 (1997).

767 47 Aken, B. L. *et al.* Ensembl 2017. *Nucleic Acids Res* **45**, D635-D642,
768 doi:10.1093/nar/gkw1104 (2017).

769 48 Zerbino, D. R. *et al.* Ensembl 2018. *Nucleic Acids Res* **46**, D754-D761,
770 doi:10.1093/nar/gkx1098 (2018).

771 49 Karolchik, D. *et al.* The UCSC Table Browser data retrieval tool. *Nucleic Acids Res* **32**,
772 D493-496, doi:10.1093/nar/gkh103 (2004).

773 50 Gramates, L. S. *et al.* FlyBase at 25: looking to the future. *Nucleic Acids Res* **45**, D663-
774 D671, doi:10.1093/nar/gkw1016 (2017).

775 51 Wernersson, R. & Pedersen, A. G. RevTrans: Multiple alignment of coding DNA from
776 aligned amino acid sequences. *Nucleic Acids Res* **31**, 3537-3539,
777 doi:10.1093/nar/gkg609 (2003).

778 52 Wernersson, R. Virtual Ribosome--a comprehensive DNA translation tool with support
779 for integration of sequence feature annotation. *Nucleic Acids Res* **34**, W385-388,
780 doi:10.1093/nar/gkl252 (2006).

781 53 Goujon, M. *et al.* A new bioinformatics analysis tools framework at EMBL-EBI.
782 *Nucleic Acids Res* **38**, W695-699, doi:10.1093/nar/gkq313 (2010).

783 54 Ronquist, F. & Huelsenbeck, J. P. MrBayes 3: Bayesian phylogenetic inference under
784 mixed models. *Bioinformatics* **19**, 1572-1574, doi:10.1093/bioinformatics/btg180
785 (2003).

786 55 Altekar, G., Dwarkadas, S., Huelsenbeck, J. P. & Ronquist, F. Parallel Metropolis
787 coupled Markov chain Monte Carlo for Bayesian phylogenetic inference.
788 *Bioinformatics* **20**, 407-415, doi:10.1093/bioinformatics/btg427 (2004).

789 56 Miller, M. A., Pfeiffer, W. & Schwartz, T. Creating the CIPRES Science Gateway for
790 inference of large phylogenetic trees. *2010 Gateway Computing Environments*
791 *Workshop (GCE)* (2010).

792 57 Di Giacomo, M., Comazzetto, S., Sampath, S. C. & O'Carroll, D. G9a co-suppresses
793 LINE1 elements in spermatogonia. *Epigenetics Chromatin* **7**, 24, doi:10.1186/1756-
794 8935-7-24 (2014).

795 58 Kim, D., Langmead, B. & Salzberg, S. L. HISAT: a fast spliced aligner with low
796 memory requirements. *Nat Methods* **12**, 357-360, doi:10.1038/nmeth.3317 (2015).

797 59 Anders, S., Pyl, P. T. & Huber, W. HTSeq--a Python framework to work with high-
798 throughput sequencing data. *Bioinformatics* **31**, 166-169,
799 doi:10.1093/bioinformatics/btu638 (2015).

800 60 Love, M. I., Huber, W. & Anders, S. Moderated estimation of fold change and
801 dispersion for RNA-seq data with DESeq2. *Genome Biol* **15**, 550, doi:10.1186/s13059-
802 014-0550-8 (2014).

803 61 Martin, M. Cutadapt removes adapter sequences from high-throughput sequencing
804 reads. *2011* **17**, 3, doi:10.14806/ej.17.1.200 (2011).

805 62 Bao, W., Kojima, K. K. & Kohany, O. Repbase Update, a database of repetitive
806 elements in eukaryotic genomes. *Mob DNA* **6**, 11, doi:10.1186/s13100-015-0041-9
807 (2015).

808 63 Langmead, B. & Salzberg, S. L. Fast gapped-read alignment with Bowtie 2. *Nat*
809 *Methods* **9**, 357-359, doi:10.1038/nmeth.1923 (2012).

810 64 Krueger, F. & Andrews, S. R. Bismark: a flexible aligner and methylation caller for
811 Bisulfite-Seq applications. *Bioinformatics* **27**, 1571-1572,
812 doi:10.1093/bioinformatics/btr167 (2011).

813 65 Kabayama, Y. *et al.* Roles of MIWI, MILI and PLD6 in small RNA regulation in mouse
814 growing oocytes. *Nucleic Acids Res* **45**, 5387-5398, doi:10.1093/nar/gkx027 (2017).
815 66 Langmead, B., Trapnell, C., Pop, M. & Salzberg, S. L. Ultrafast and memory-efficient
816 alignment of short DNA sequences to the human genome. *Genome Biol* **10**, R25,
817 doi:10.1186/gb-2009-10-3-r25 (2009).

818

819 **Extended Data figure legends**

820

821 **Extended Data Figure 1 | Expression pattern and presence of nuclear localization signals** 822 **for novel MIWI2 interactors.**

823 **a, b**, Relative expression of indicated transcripts as measured by Affymetrix microarray in
824 E16.5 gonocytes (n=2), adult spermatogonia (n=3), spermatocytes (n=3), MEFs (n=3) and
825 bone marrow (n=2). Data are mean and s.e.m. NLS indicates presence of a nuclear localization
826 signal as predicted by cNLS mapper.

827

828 **Extended Data Figure 2 | Homology alignment of SPOCD1 SPOC and TFIIS-M domains.**

829 **a**, Multiple sequence alignment of the SPOC domain from SPOCD1 with representative
830 vertebrate sequences from PHF3, DIDO1 and SPEN orthologues. The numbering for mouse
831 SPOCD1 is shown above. Secondary structure elements for the human SHARP SPOC domain
832 (PDBid 1OW1, SHARP is the human SPEN orthologue) are shown below the sequence, with
833 dark rectangles for alpha helices and lighter arrows for beta strands. **b**, Multiple sequence
834 alignment of TFIIS-M domain of SPOCD1 with equivalent sequences from TFIIS, PHF3 and
835 DIDO1. Secondary structure elements from human PHF3 (PDBid 2DME) and human TFIIS
836 (PDBid 3NDQ) are shown below, using the same annotation as in (a). Sequences are coloured
837 according to sequence identity.

838

839 **Extended Data Figure 3 | Phylogeny of SPOCD1.**

840 Bayesian phylogeny of *Spocd1* (blue) and its vertebrate paralogs *Phf3* (red) and *Dido1* (green)
841 inferred from cDNA sequences. Posterior probabilities of splits are shown as node labels.
842 Branch lengths measure the expected substitutions per site as indicated in the scale bar.

843

844 **Extended Data Figure 4 | Generation and characterisation of the *Spocd1*^{null} mouse allele.**

845 **a**, Schematic representation of the *Spocd1* locus and the encoded 1015 amino acids (aa) protein
846 (transcript XM_017320505.1) as well as design of the sgRNA targeting *Spocd1* exon 7, which
847 harbours part of the TFIIS-M domain. **b**, Schematic representation and sequencing trace
848 (lower) of the part of *Spocd1*^{null} exon 7 harbouring the mutation site. The mutated site,
849 highlighted in red, contains 2 premature stop codons and causes a frame-shift. Sequencing was
850 repeated with identical results on n=3 animals. **c**, Representative image of genotyping results
851 for *Spocd1*^{+/+}, *Spocd1*^{+/-} and *Spocd1*^{-/-} animals. Similar results were obtained for all animals of
852 the *Spocd1*⁻ line. **d**, Number of E16.5 embryos per plug from matings of mice with the indicated
853 *Spocd1* genotypes are presented. Mean and s.e.m. from n=7 *Spocd1*^{+/+} dams mated to n=3
854 *Spocd1*^{+/+} studs and n=12 *Spocd1*^{-/-} dams mated to n=5 *Spocd1*^{+/-} studs is plotted. NS, non-
855 significant difference (P~0.98), two-tailed Student's t-test. **e**, Representative PAS and
856 haematoxylin stained histological testis sections of different stages of the seminiferous cycle
857 are shown of (n=3) *Spocd1*^{+/+} and *Spocd1*^{-/-} animals, indicating a germ cell differentiation arrest
858 at the early pachytene stage. Scale bar, 5 µm. eP, early pachytene; RS, round spermatids, eS(13)
859 elongating spermatids (step 13); PL, pre-leptotene; P, pachytene; L, leptotene; Z, zygotene;
860 m2, secondary meiocytes. **f**, Representative images of zygotene spermatocytes in wildtype and
861 *Spocd1*^{-/-} adult testis sections stained for the synaptonemal complex proteins SCP1 (red) and
862 SCP3 (green). DNA stained with DAPI (blue). Scale bar, 1 µm. The representative images

863 presented in panels e and f are from n=3 mice per genotype. **g, h** Analysis of TE expression in
864 P20 testes from n=3 wildtype, *Spocd1*^{-/-} and *Miwi2*^{-/-} mice by RNA-seq. **g**, Comparison of TE
865 expression in *Miwi2*^{-/-} and wildtype testes is shown. TEs with a significantly different (P<0.01,
866 Benjamini-Hochberg adjusted two-sided Wald's test) change in expression (>2-fold) are
867 highlighted in red and the top 12 most up-regulated TEs in *Miwi2*^{-/-} testes are labelled. **h**,
868 Comparison of TE expression in *Spocd1*^{-/-} and wildtype testes is shown. TEs with a
869 significantly different (P<0.01, Benjamini-Hochberg adjusted two-sided Wald's test) change
870 in expression (>2-fold) are highlighted in red and same TEs as in (a) are labelled. **i**, Comparison
871 of TE expression in *Spocd1*^{-/-} and *Miwi2*^{-/-} testes is shown. TEs with a significantly different
872 (P<0.01, Benjamini-Hochberg adjusted two-sided Wald's test) change in expression (>2-fold)
873 are highlighted in red. TEs which are significantly up-regulated in *Miwi2*^{-/-} relative to wildtype
874 are highlighted in black.

875

876 **Extended Data Figure 5 | CpG Methylation analysis of different genomic features and TE**
877 **families.**

878 Analysis of genomic CpG methylation of undifferentiated P14 spermatogonia from (n=3)
879 wildtype, *Spocd1*^{-/-} and *Miwi2*^{-/-} mice is presented. **a, b**, Scatter plots comparing CpG
880 methylation levels for the respective genomic features between wildtype and *Spocd1*^{-/-} or
881 *Miwi2*^{-/-} (**a**) and between *Spocd1*^{-/-} or *Miwi2*^{-/-} spermatogonia (**b**) are shown. **c, d**, Scatter plots
882 comparing CpG methylation levels for the respective TE families between wildtype and
883 *Spocd1*^{-/-} or *Miwi2*^{-/-} (**c**) and between *Spocd1*^{-/-} or *Miwi2*^{-/-} spermatogonia (**d**) are shown. Data
884 is mean from n=3 biological replicates per genotype and shown as individual data points (grey)
885 overlaid by a density map.

886

887 **Extended Data Figure 6 | Methylation analysis of TE families.**

888 Analysis of genomic CpG methylation of undifferentiated P14 spermatogonia from (n=3)
889 wildtype, *Spocd1*^{-/-} and *Miwi2*^{-/-} mice is presented. **a**, Metaplots of CpG methylation over
890 L1Md_A, IAPey and MMERVK10C elements and adjacent 2 kb are shown. Schematic
891 representation of the element is shown below. **b**, Metaplots of mean CpG methylation over
892 LINE1 elements and adjacent 1 kb are shown. The Methyl-seq datasets of P14 wildtype, *Miwi2*^{-/-}
893 ^{-/-} and *Spocd1*^{-/-} spermatogonia are compared to WGBS datasets of adult *Mili*^{-/-} spermatocytes
894 (Molaro et al. 2014⁴) and P10 *Dnmt3c*^{+/-}, *Dnmt3c*^{-/-}, *Dnmt3l*^{+/-}, *Dnmt3l*^{-/-} germ cells (Barau et
895 al. 2016¹²). Schematic representation of LINE1 is shown below. **c**, Correlation analysis of mean
896 CpG methylation loss relative to wildtype over individual elements of the indicated TE family
897 in relation to their divergence from the consensus sequence is shown for *Miwi2*^{-/-} and *Spocd1*^{-/-}
898 ^{-/-} spermatogonia.

899

900 **Extended Data Figure 7 | piRNA analysis.**

901 piRNA analyses of small RNAs sequenced from E16.5 testis from (n=3) *Spocd1*^{+/-} and *Spocd1*^{-/-}
902 ^{-/-} mice are presented. **a**, Relative frequency of piRNAs mapping to LINE1 and IAP families
903 from *Spocd1*^{+/-} and *Spocd1*^{-/-} E16.5 testes. Plots are shown for all piRNA or anti-sense piRNAs.
904 Data are mean and s.e.m. Adjusted P-values are listed, P=1.0 values are denoted as NS
905 (Bonferroni adjusted two-sided Student's t-test). **b**, Scatter plots showing mean expression of
906 all (n=124411) piRNAs. The identity line is shown in red. r, Pearson's correlation coefficient.
907 **c**, Nucleotide features of piRNA from *Spocd1*^{+/-} and *Spocd1*^{-/-} E16.5 testes. Frequency of
908 mapped piRNAs with a U at position 1 (1U) and with an A at position 10 (10A) are shown for
909 L1Md_T elements. Data represent the mean and s.e.m. Adjusted P-values are shown
910 (Bonferroni adjusted two-sided Student's t-test) **d**, Ping-pong analysis of piRNAs from
911 *Spocd1*^{+/-} and *Spocd1*^{-/-} E16.5 testis. Relative frequencies of the distances between 5' ends of
912 complementary piRNAs are shown for the indicated LINE1 and IAP families. **e**, Nucleotide

913 features of piRNA from *Spocd1*^{+/-} and *Spocd1*^{-/-} E16.5 testis. Relative frequencies of piRNAs
914 with a U at position 1 (1U) and with an A at position 10 (10A) are shown for respective
915 elements shown in (d). Data are mean and s.e.m. Adjusted P-values are listed, P=1.0 values
916 denoted as NS (Bonferroni adjusted two-sided Student's t-test) **f**, Positions of piRNAs mapped
917 to the consensus sequence of LIMd_T. Positive and negative values indicate sense and
918 antisense piRNAs, respectively. Schematic representation of LIMd_T is shown above.

919

920 **Extended Data Figure 8 | TE and gene expression in *Spocd1*^{-/-} gonocytes.**

921 Analysis of TE and gene expression in E16.5 *Spocd1*^{+/-} and *Spocd1*^{-/-} gonocytes by RNA-seq
922 from n=3 mice per genotype. **a**, Comparison of TE expression in *Spocd1*^{+/-} and *Spocd1*^{-/-}
923 gonocytes is shown. TEs up-regulated in *Miwi2*^{-/-} testes at P20 are highlighted in black. **b**,
924 Comparison of gene expression in *Spocd1*^{+/-} and *Spocd1*^{-/-} gonocytes is shown. Significantly
925 expressed genes (P<0.01, Benjamini-Hochberg adjusted two-sided Wald's test, >2-fold
926 change) are highlighted in red.

927

928 **Extended Data Figure 9 | Generation of the *Spocd1*^{HA} mouse allele.**

929 **a**, Schematic representation of the SPOCD1 protein and *Spocd1* locus as well as design of the
930 sgRNA targeting the 3' UTR near the translation termination site on *Spocd1* exon 15. The
931 *Spocd1*^{HA} allele encodes for a carboxy-terminal GGGGS linker followed by the HA epitope
932 tag. The protospacer adjacent motif (PAM) site was mutated to inhibit re-targeting of the
933 *Spocd1*^{HA} allele by the sgRNA-CAS9 complex. All inserted nucleotides and corresponding
934 encoded amino acids are highlighted in red. The SPOCD1-HA protein is shown as a schematic
935 representation. **b**, Schematic representation of the targeting strategy to generate the *Spocd1*^{HA}
936 allele with a short single stranded DNA oligo donor (ssODN) of 200 nucleotides containing 5'
937 and 3' homology arms (5'HA and 3'HA) of 72 nucleotides. **c**, Representative image of

938 genotyping results for *Spocd1*^{+/+}, *Spocd1*^{HA/+} and *Spocd1*^{HA/HA} animals. Similar results were
939 obtained for all animals of the *Spocd1*^{HA} line. **d**, Sequencing trace of part of a PCR amplicon
940 of the HA epitope tag insertion site from a *Spocd1*^{HA/HA} animal. The experiment was repeated
941 with identical results on n=2 animals. **e, f, g**, Representative images of wildtype (**e**), *Spocd1*^{HA/+}
942 (**f**) and *Miwil2*^{HA/+} (**g**) testis sections at the indicated developmental time point probed with anti-
943 HA antibody in green. DNA stained with DAPI in blue. Scale bars, 10 μ m. The representative
944 images presented in panels e to g are from experiments done n=3 mice as biological replicates
945 with similar results.

946

947 **Extended Data Figure 10 | Co-immunoprecipitation experiments of SPOCD1 and**
948 **DNMT3A/L/C in HEK cells.**

949 Western blot analysis of co-immunoprecipitation of SPOCD1-HA with DNMT3L-FLAG,
950 DNMT3A-FLAG, DNMT3C-FLAG or GFP in HEK cells. Shown are lysate sample (L),
951 control IP (protein G beads) (B) and anti-HA IP (IP) for 4 experiments. For uncropped source
952 data, see Supplementary Figure 1.

953

Figure 1

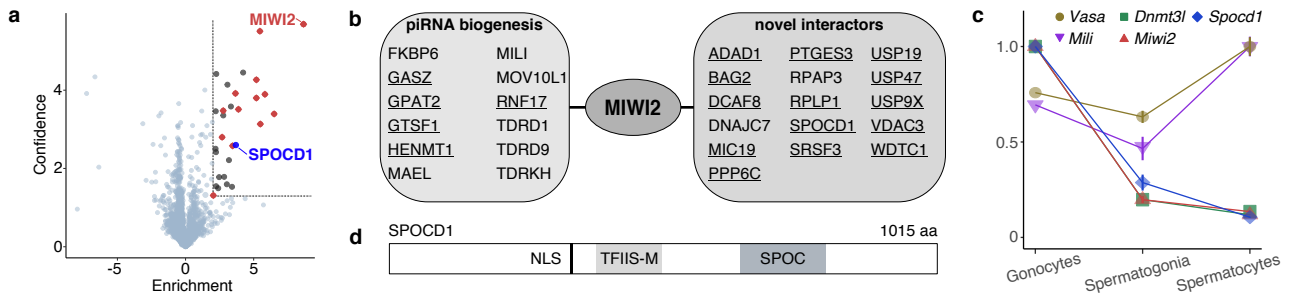


Figure 2

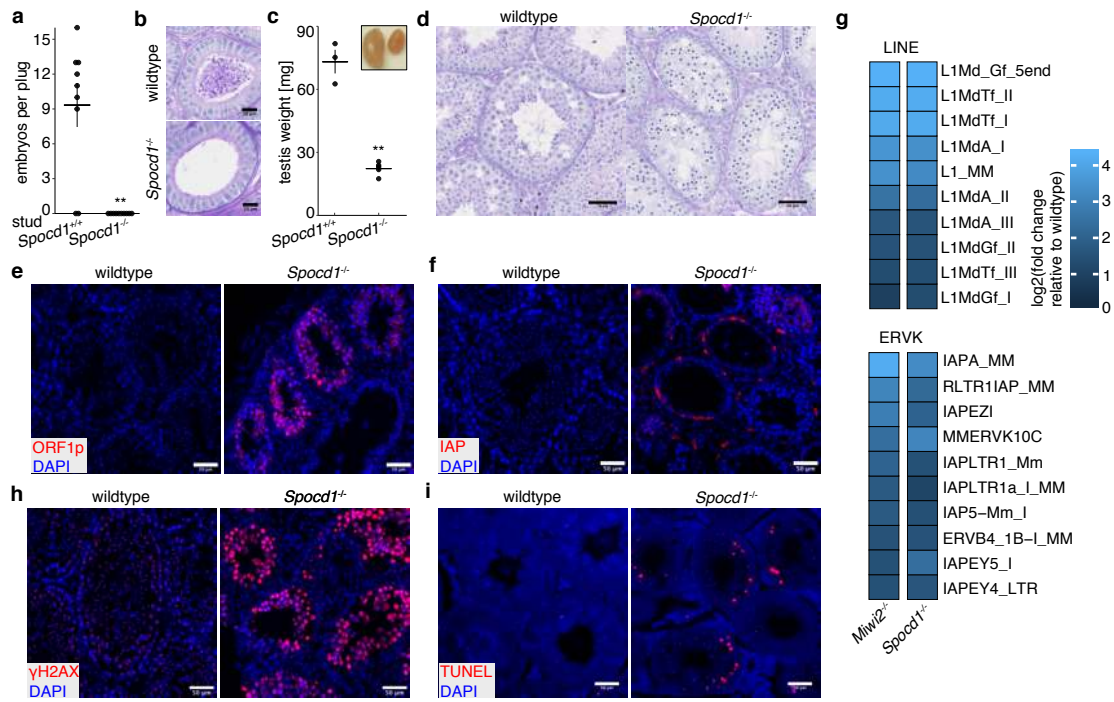


Figure 3

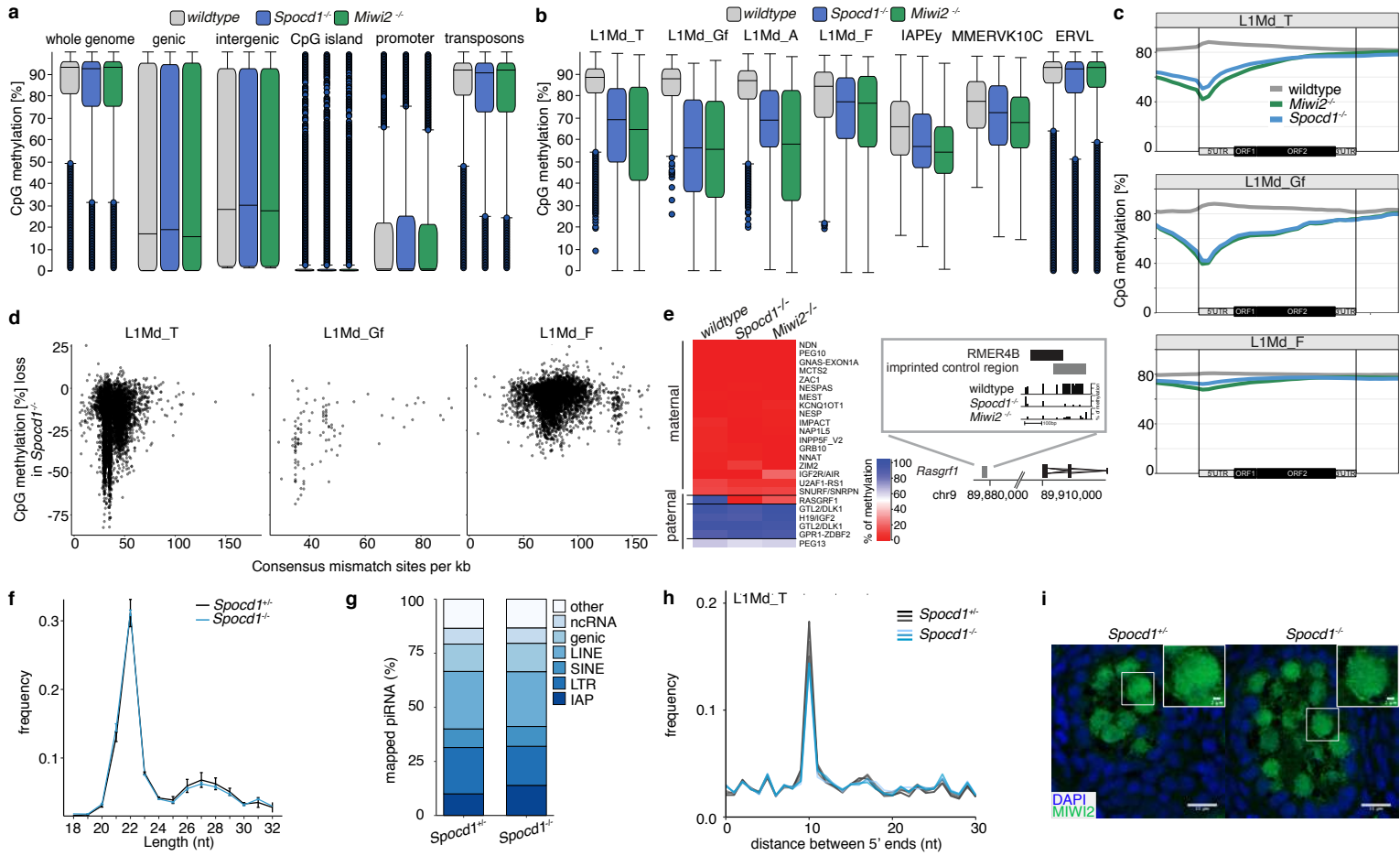
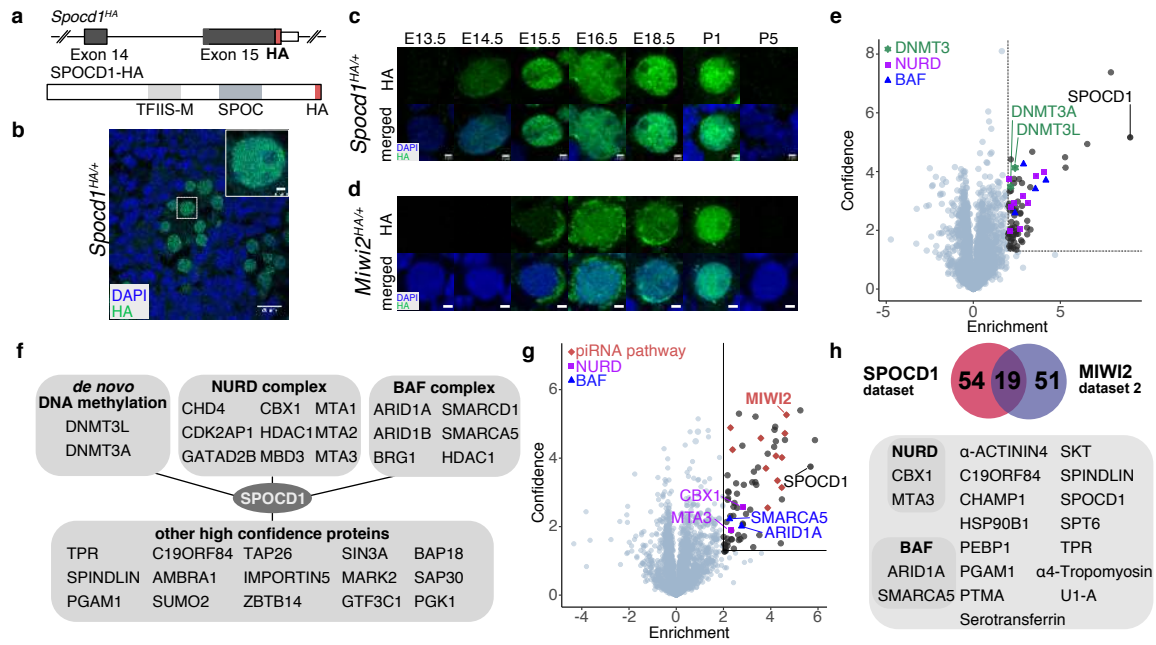
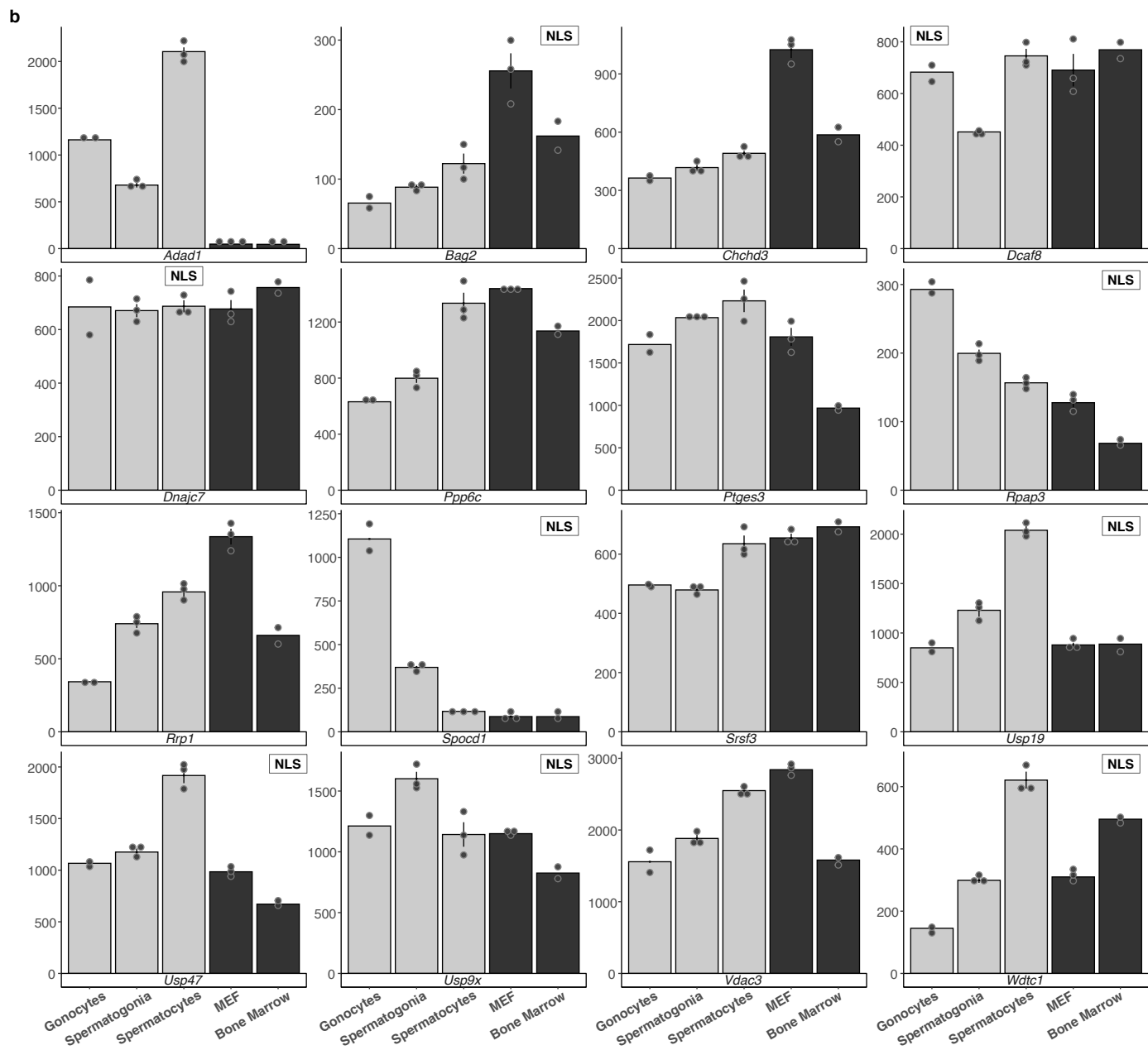
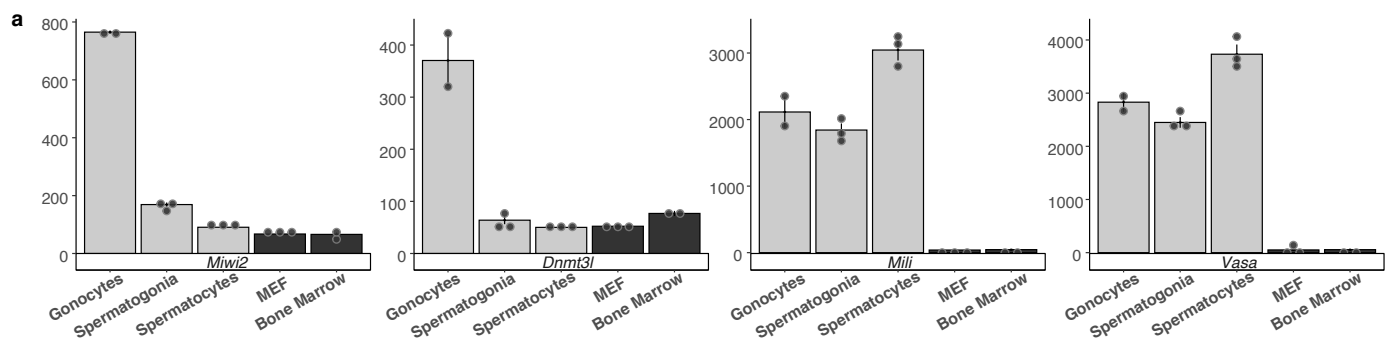


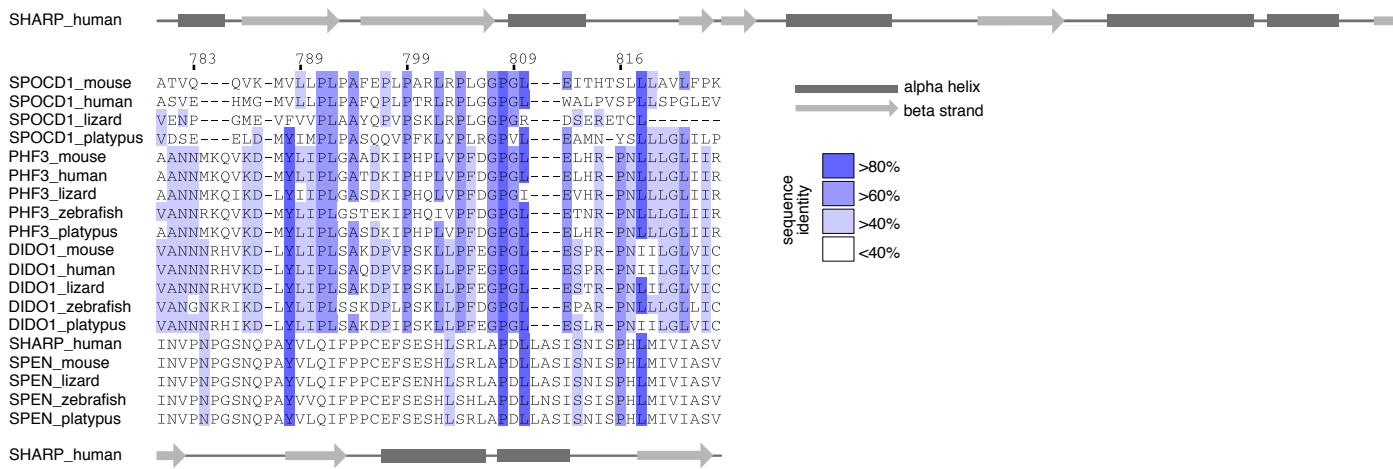
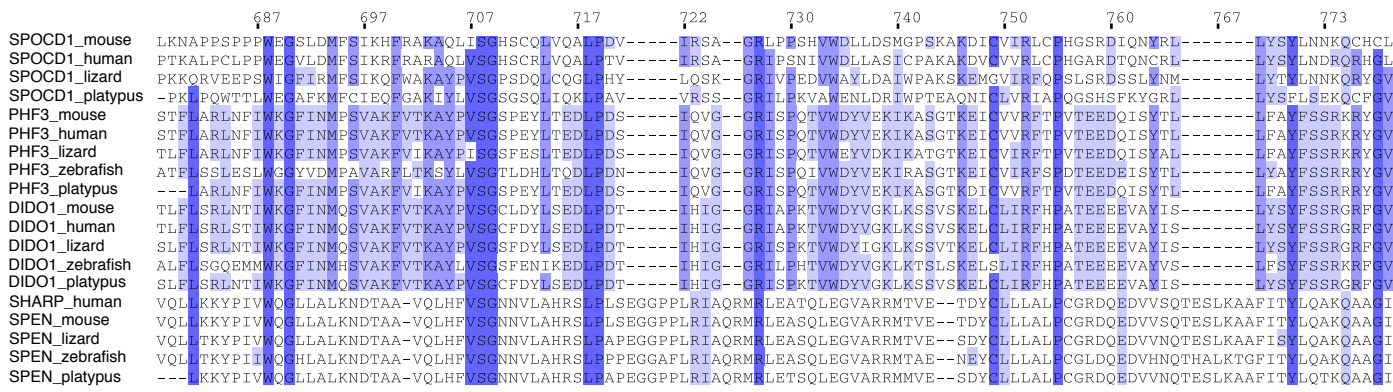
Figure 4



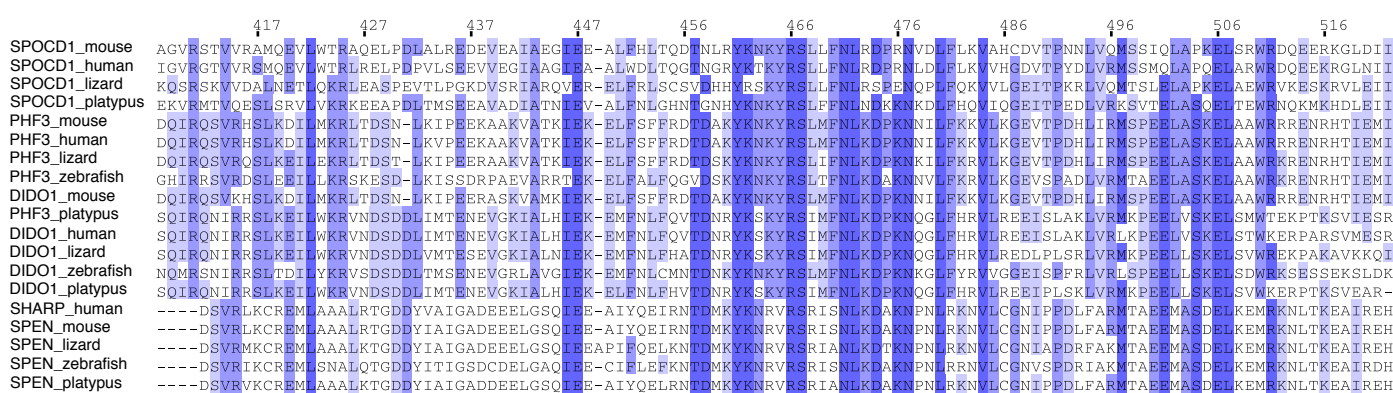
Extendend Data



a SPOC domain



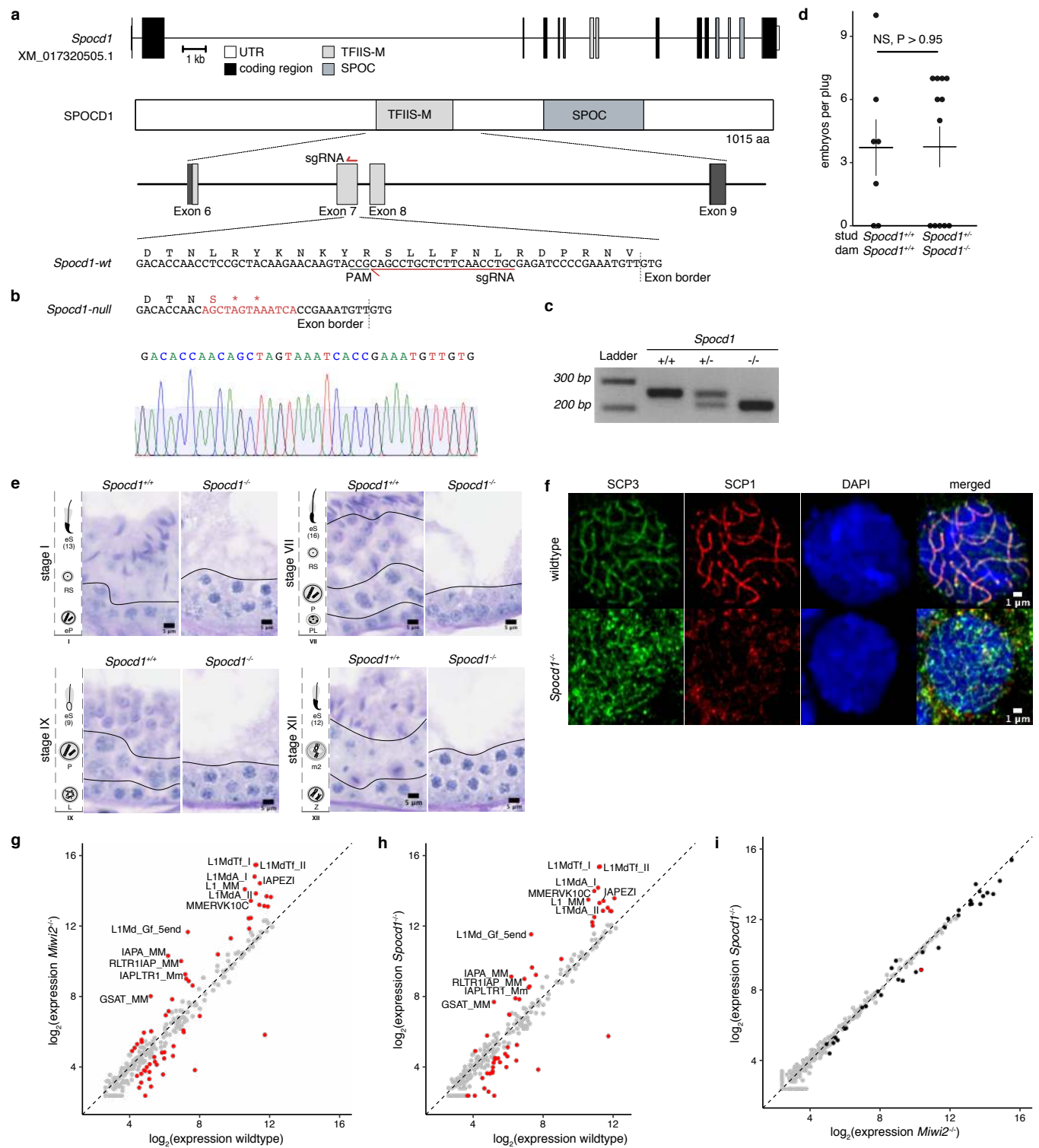
b TFIIIS-M domain

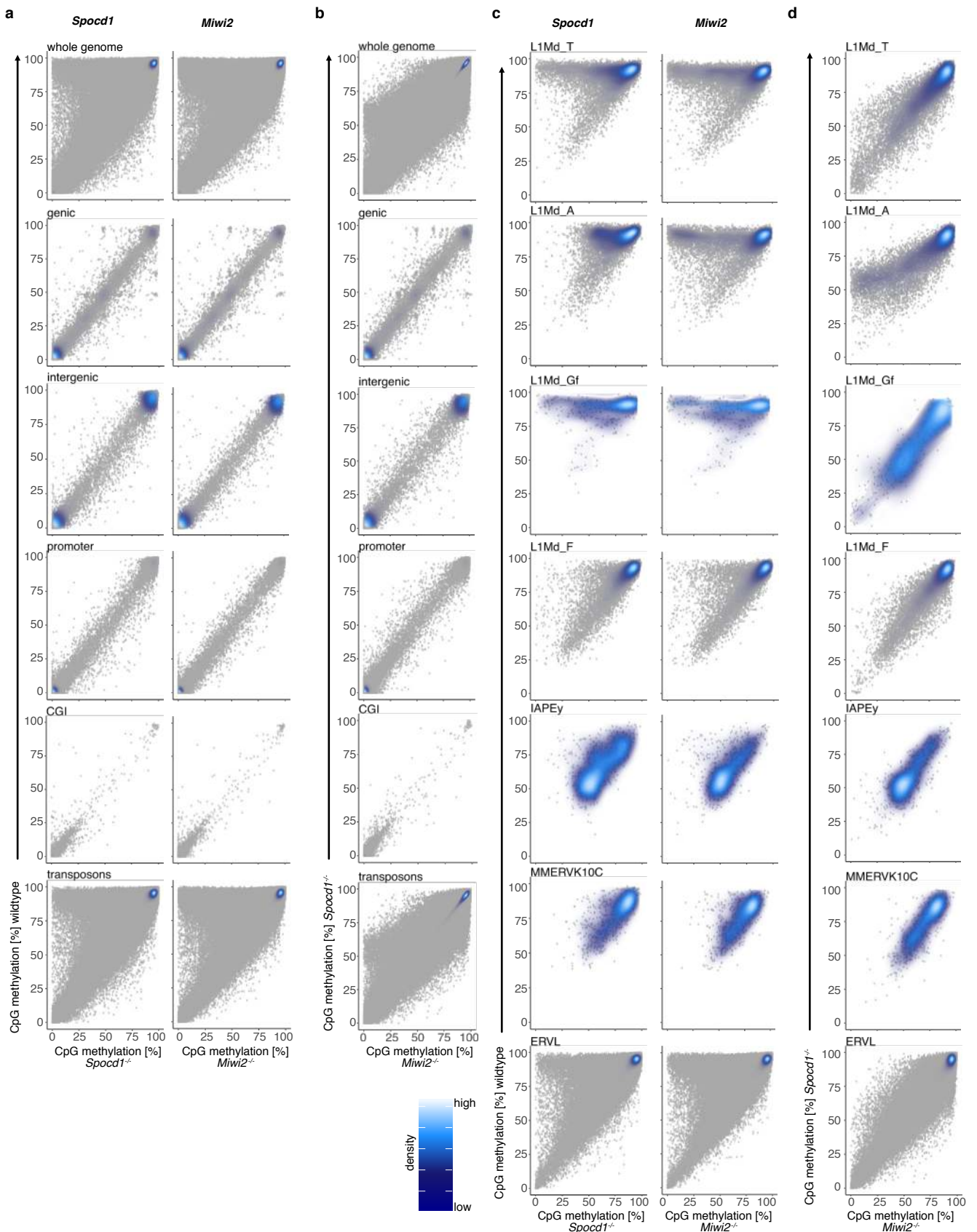


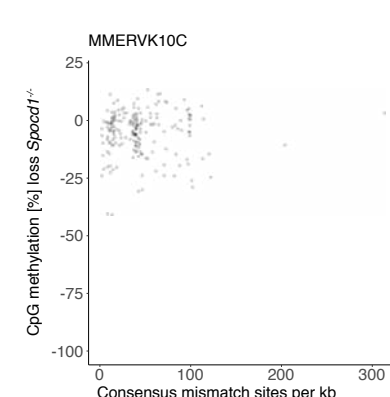
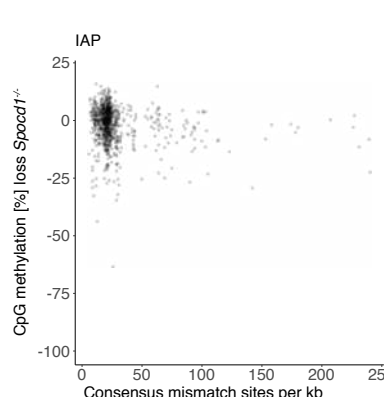
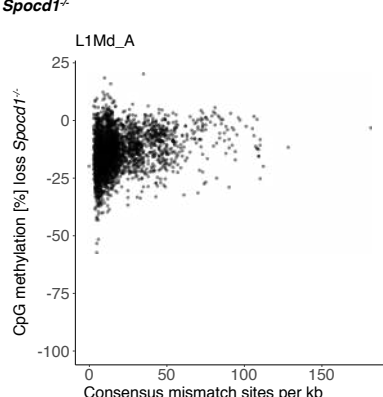
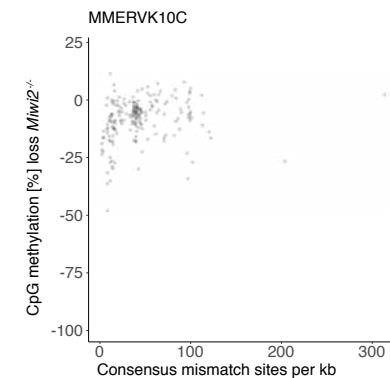
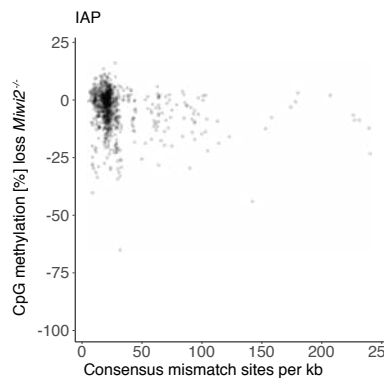
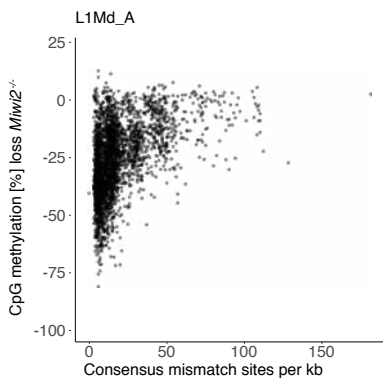
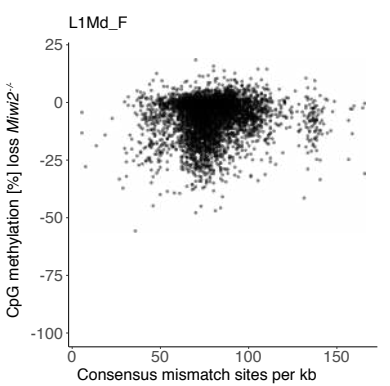
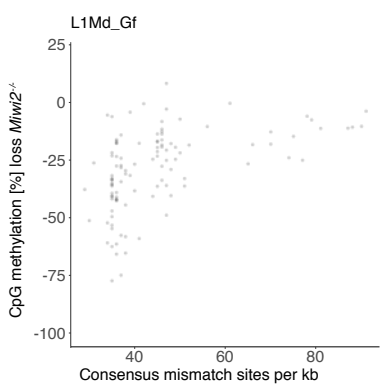
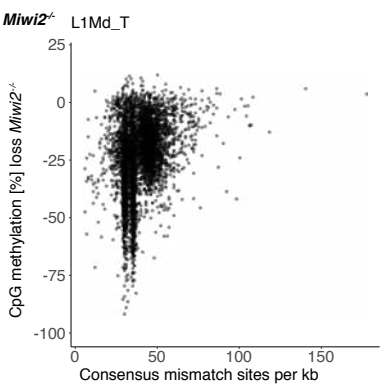
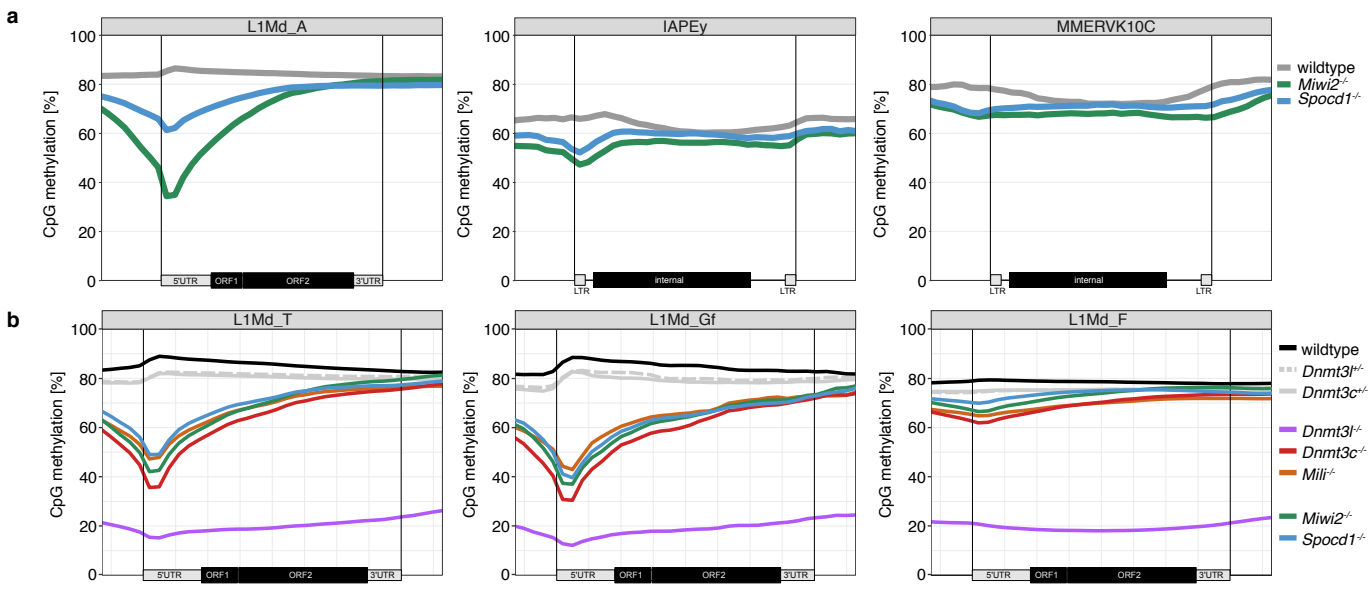


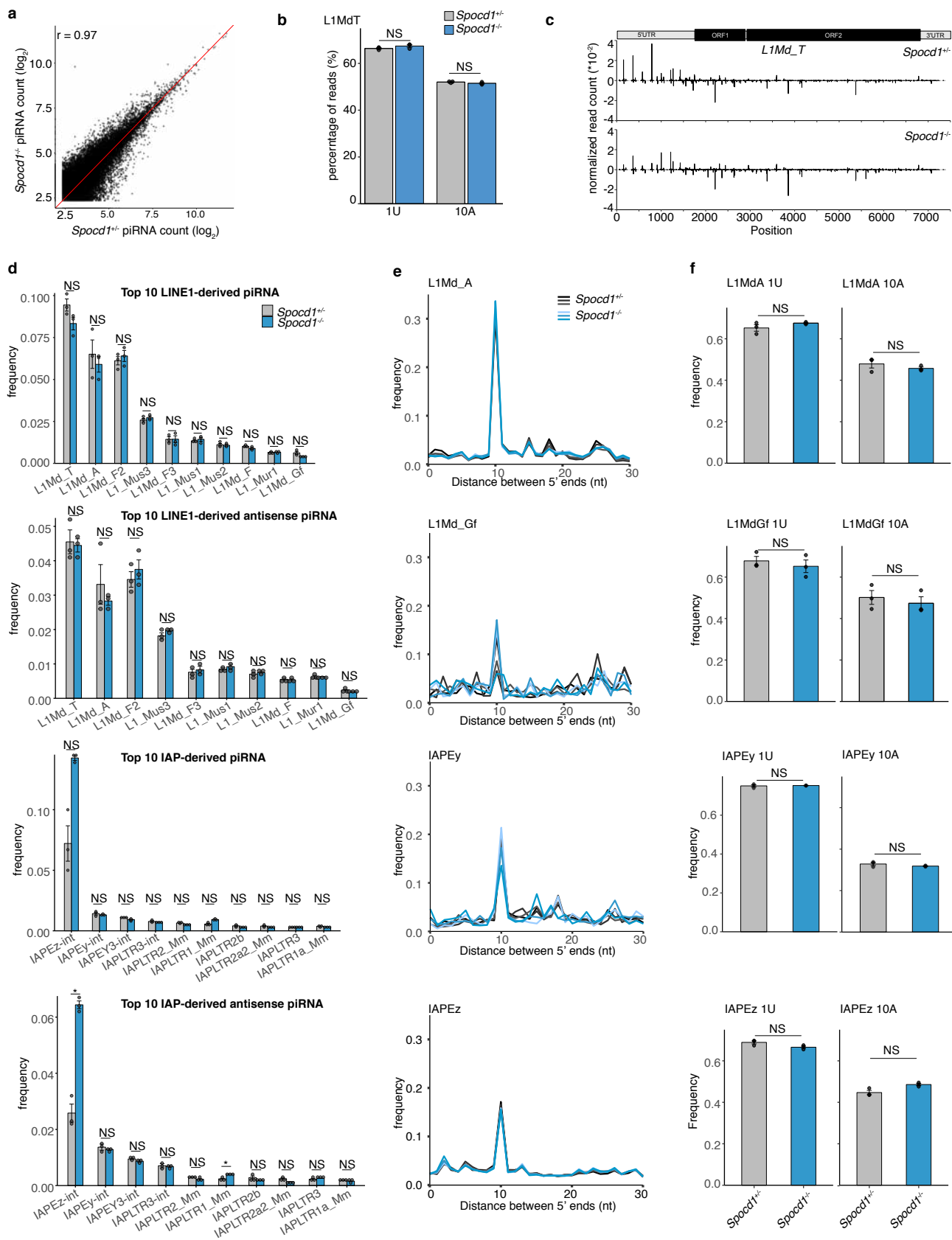
set-5 | *Caenorhabditis elegans*

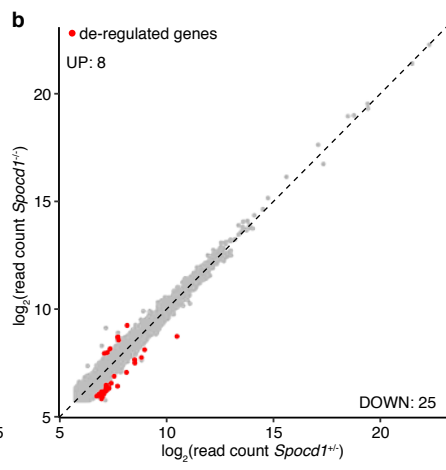
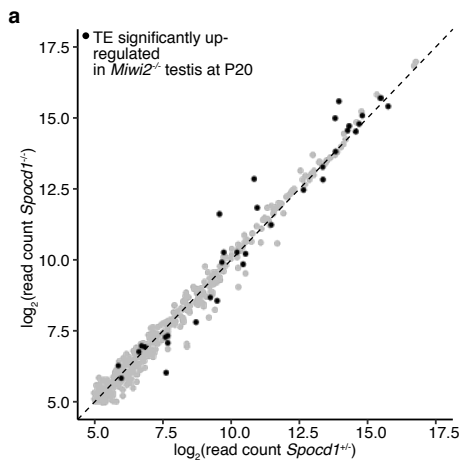
0.4

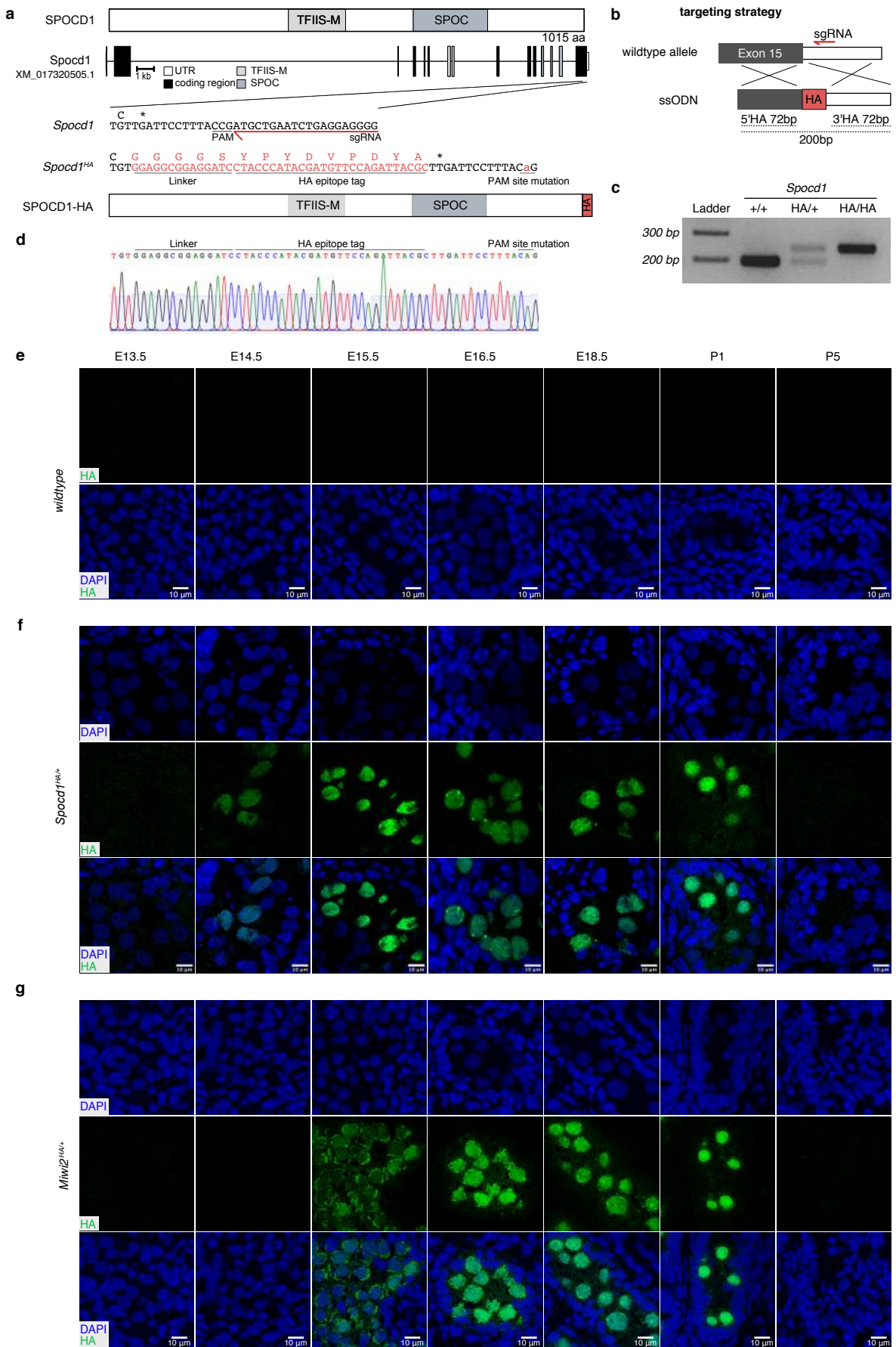


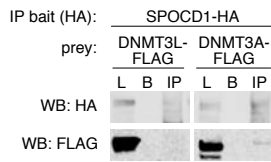
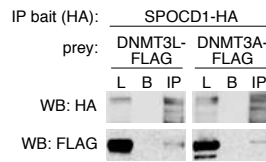
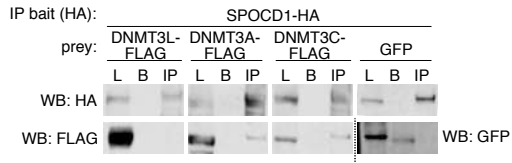
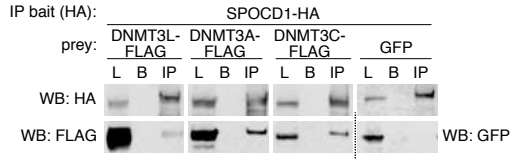






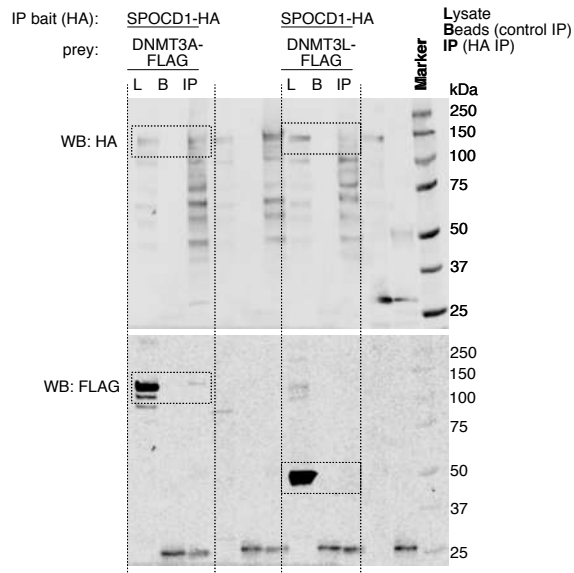




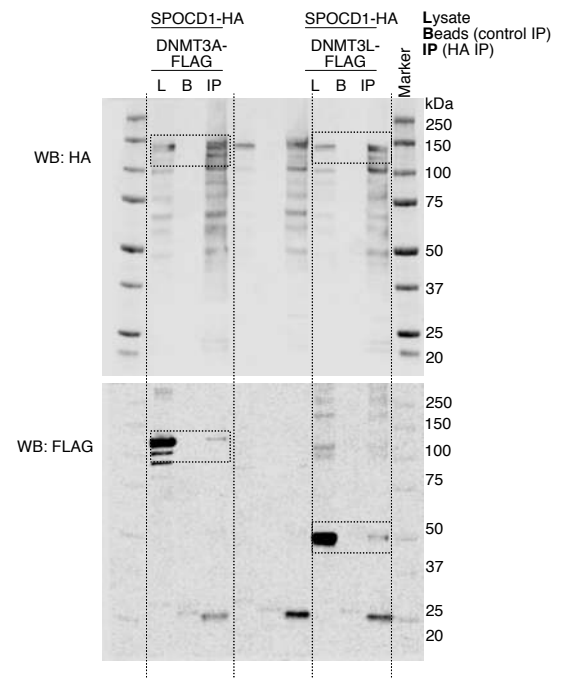
Experiment 1**Experiment 2****Experiment 3****Experiment 4**

Supplementary Figure 1

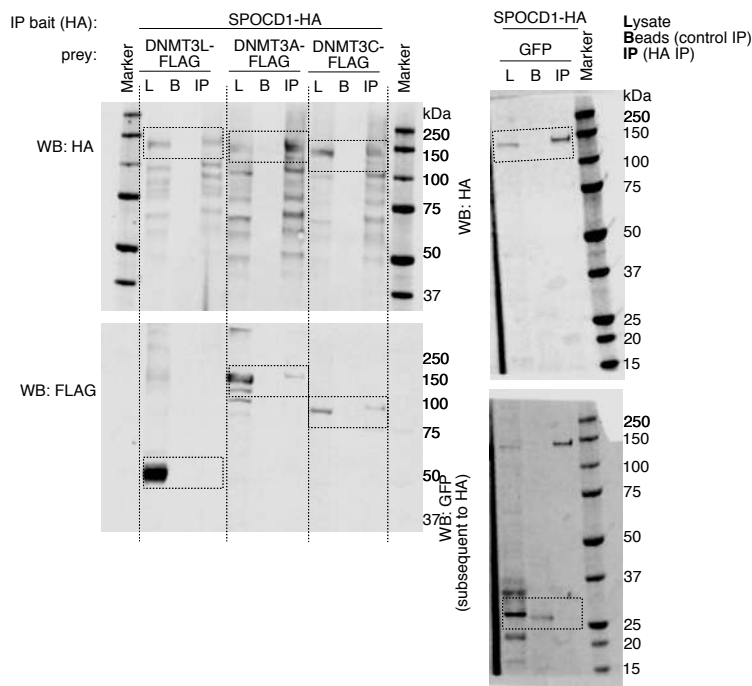
Experiment 1



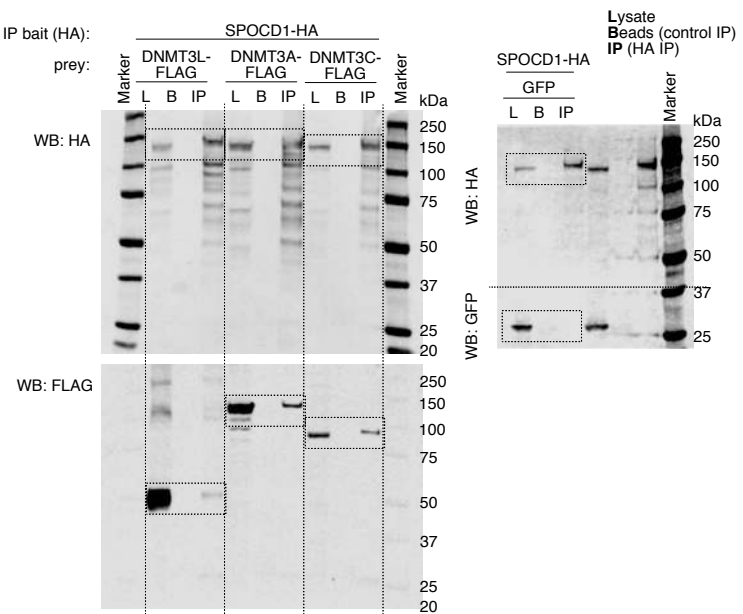
Experiment 2



Experiment 3

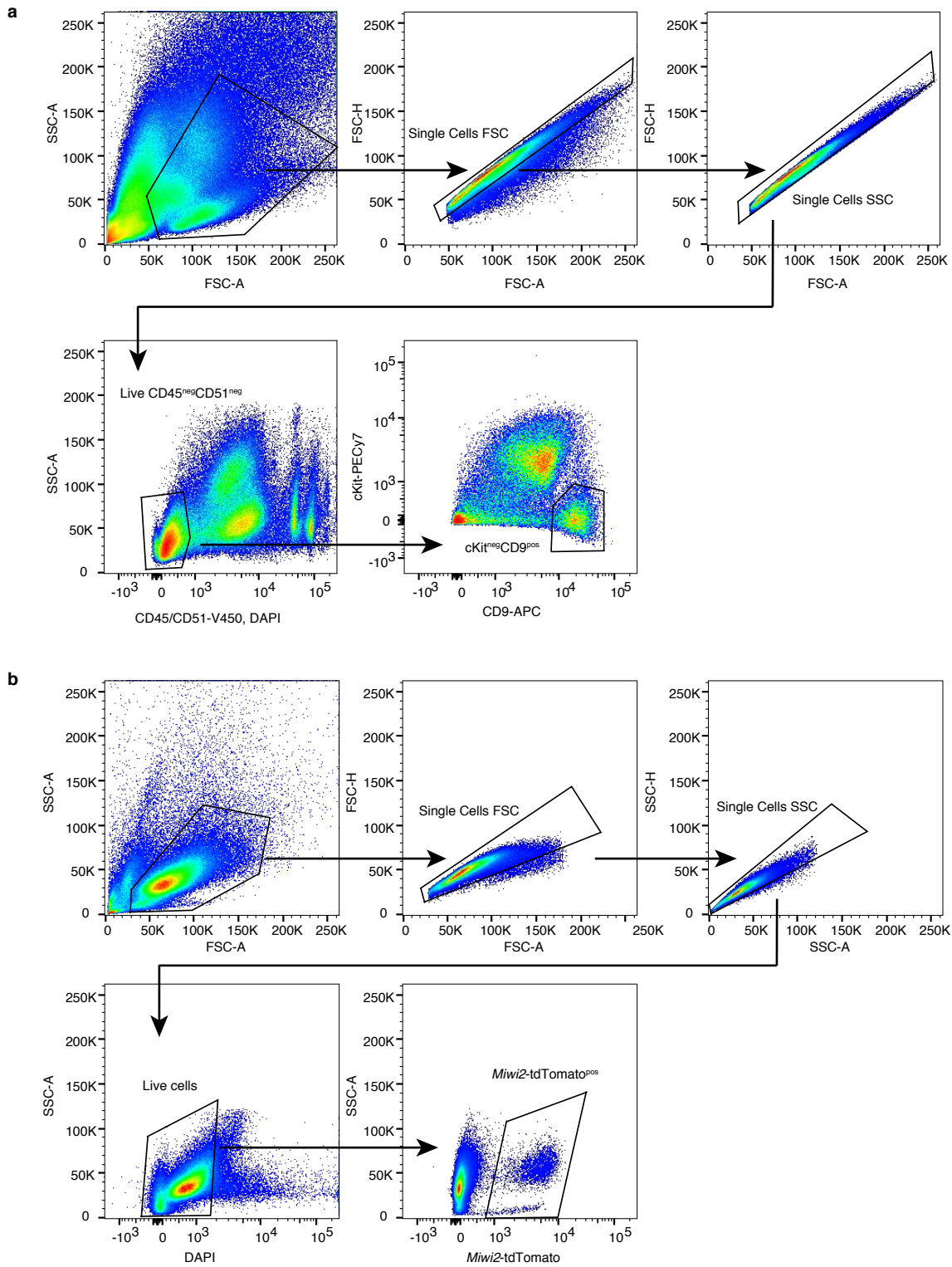


Experiment 4



Supplementary Figure 1 | Uncropped Western blot images

Uncropped source data of experiments shown in Extended Data Figure 10: Western blot analysis of co-immunoprecipitation of SPOCD1-HA with DNMT3L-FLAG, DNMT3A-FLAG, DNMT3C-FLAG or GFP in HEK cells. Shown are lysate sample (L), control IP (protein G beads) (B) and anti-HA IP (IP) for 4 experiments.



Supplementary Figure 2 | FACS Gating strategy

a, FACS isolation of post-natal day 14 (P14) undifferentiated spermatogonia. Representative example of a gating strategy for sorting live CD45^{neg}CD51^{neg}c-Kit^{pos}CD9^{pos} undifferentiated spermatogonia from P14 mice, where a single-cell suspension of testicular cells was stained with anti-CD45^{biotin}, anti-CD51^{biotin}, anti-c-Kit^{PE-Cy7} and anti-CD9^{APC} antibodies as well as streptavidin^{V450} and DAPI. A representative experiment of n=3 mice is shown. **b**, FACS isolation of E16.5 foetal gonocytes using the *Miwi2*^{tdTOM} reporter allele. Representative example of a gating strategy for sorting live *Miwi2*-tdTomato^{pos} gonocytes from E16.5 mice, where a single-cell suspension of testicular cells was stained with DAPI. A representative experiment of n=3 mice is shown.

Supplementary Table 1

protein.ID	protein	gene	P-value	fold-enrichment
Q8CGT6	MIWI2	<i>Piwi4</i>	2.1E-06	404.5
Q91XW8	FKBP6	<i>Fkbp6</i>	3.1E-06	44.0
E9Q9M5	USP19	<i>Usp19</i>	3.5E-05	18.7
D3Z7C6	PTGES3	<i>Ptges3</i>	3.8E-05	4.8
Q14BI7	TDRD9	<i>Tdrd9</i>	5.4E-05	36.8
Q8N7N5	DCAF8	<i>Dcaf8</i>	7.2E-05	8.4
Q14DK4	GPAT2	<i>Gpat2</i>	1.1E-04	9.0
Q99MV7	RNF17	<i>Rnf17</i>	1.2E-04	12.7
A0A0G2JFB2	TDRKH	<i>Tdrkh</i>	1.3E-04	56.8
F2YMC1	MOV10L1	<i>Mov10l1</i>	1.6E-04	36.7
Q9D706	RPAP3	<i>Rpap3</i>	2.6E-04	10.1
Q8VD46	GASZ	<i>Asz1</i>	3.1E-04	14.8
D3YUE6	GTSF1	<i>Gtsf1</i>	3.3E-04	6.8
Q91YN9	BAG2	<i>Bag2</i>	3.4E-04	4.7
Q80ZK9	WDTC1	<i>Wdtd1</i>	4.4E-04	6.8
Q8CAE2	HENMT1	<i>Henmt1</i>	7.3E-04	45.0
Q99MV1	TDRD1	<i>Tdrd1</i>	1.6E-03	6.4
B1ASB6	SPOCD1	<i>Spocd1</i>	2.4E-03	12.6
Q8CDG1	MILI	<i>Piwi2</i>	2.6E-03	11.0
A0A0N4SVL9	PPP6C	<i>Ppp6c</i>	3.1E-03	4.6
Q58E35	RPLP1	<i>Rplp1</i>	3.8E-03	4.7
Q9CRB9	MIC19	<i>Chchd3</i>	6.1E-03	9.1
Q3TX38	VDAC3	<i>Vdac3</i>	1.6E-02	7.1
Q5SUE7	ADAD1	<i>Adad1</i>	1.7E-02	5.5
Q3U781	SRSF3	<i>Srsf3</i>	2.5E-02	8.2
Q3UL32	DNAJC7	<i>Dnajc7</i>	2.8E-02	4.7
Q8BY87	USP47	<i>Usp47</i>	2.9E-02	10.7
Q4FE56	USP9X	<i>Usp9x</i>	3.2E-02	5.3
Q8BVN9	MAEL	<i>Mael</i>	4.9E-02	4.1

Supplementary Data Table 1 | Proteins identified as MIWI2 interactors.

Table listing all statistically significant ($P < 0.05$, two-sided Student's t-test, $n=3$) proteins that are at least 4-fold enriched in the HA-MIWI2 immuno-precipitation.

Supplementary Table 2

TE	fold-change	P-value
IAPA_MM	5.09	8.72E-05
RLTR1IAP_MM	4.67	1.25E-07
IAPEZI	3.52	1.85E-05
IAPLTR1a_I_MM	2.46	2.65E-04
ERV4_1B-I_MM	0.48	5.69E-11
IAPEY5_LTR	0.48	9.05E-04
RLTR6I_MM	0.43	7.46E-12
ERV4_2-I_MM	0.39	9.74E-06
RLTR10B2	0.39	1.07E-11
MURVY-int	0.38	3.74E-04
ERV2_1A-I_MM	0.30	6.34E-09
ZP3AR	0.26	3.19E-11
ERV4_3-I_MM	0.19	4.55E-06

Supplementary Data Table 2 | Deregulated TEs in E16.5 *Spocd1*^{-/-} gonocytes.

Table of all statistically significant ($P < 0.01$, Benjamini-Hochberg adjusted two-sided Wald's test), deregulated (>2 -fold) TEs identified in E16.5 *Spocd1*^{-/-} gonocytes, listing fold-change of expression (relative to wildtype) and P-values as determined from RNA-seq data. $n=3$ for both genotypes.

Supplementary Table 3

ensemble ID	gene_name	fold-change	P-value
ENSMUSG00000058267	<i>Mrps14</i>	3.02	1.23E-03
ENSMUSG00000034544	<i>Rsrc1</i>	2.69	2.11E-05
ENSMUSG00000041923	<i>Nol4</i>	2.66	1.09E-05
ENSMUSG00000031099	<i>Smarca1</i>	2.63	9.75E-07
ENSMUSG00000026748	<i>Plxdc2</i>	2.50	2.07E-03
ENSMUSG00000010721	<i>Lmbr1</i>	2.48	4.96E-04
ENSMUSG00000072774	<i>Zfp951</i>	2.39	2.30E-04
ENSMUSG00000023087	<i>Noct</i>	2.29	7.60E-03
ENSMUSG00000004668	<i>Abca13</i>	0.44	2.61E-05
ENSMUSG00000037747	<i>Phyhipl</i>	0.40	1.11E-05
ENSMUSG00000025014	<i>Dntt</i>	0.35	6.42E-03
ENSMUSG00000079173	<i>Zan</i>	0.33	3.55E-06
ENSMUSG00000036526	<i>Card11</i>	0.33	9.75E-07
ENSMUSG00000030259	<i>Rassf8</i>	0.28	8.21E-04
ENSMUSG00000028784	<i>Spocd1</i>	0.25	1.40E-18
ENSMUSG00000030577	<i>Cd22</i>	0.24	9.26E-03
ENSMUSG00000031022	<i>BC051019</i>	0.23	8.10E-03
ENSMUSG00000074277	<i>Phldb3</i>	0.22	4.09E-04
ENSMUSG00000036634	<i>Mag</i>	0.18	8.08E-03
ENSMUSG00000078234	<i>Klhdc7a</i>	0.13	3.49E-05
ENSMUSG00000002980	<i>Bcam</i>	0.11	1.69E-06
ENSMUSG00000114818	<i>Gm35164</i>	0.11	4.96E-04
ENSMUSG00000083767	<i>Gm11405</i>	0.10	1.59E-03
ENSMUSG00000109613	<i>Gm45405</i>	0.10	1.77E-13
ENSMUSG00000068758	<i>Il3ra</i>	0.09	1.85E-06
ENSMUSG00000066361	<i>Serpina3c</i>	0.07	1.45E-04
ENSMUSG00000109326	<i>Gm9165</i>	0.06	8.95E-04
ENSMUSG00000090126	<i>4930519F09Rik</i>	0.06	1.42E-04
ENSMUSG00000040525	<i>Cblc</i>	0.06	8.21E-04
ENSMUSG00000085658	<i>Gm15704</i>	0.06	5.15E-06
ENSMUSG00000082398	<i>Gm11927</i>	0.04	3.90E-03
ENSMUSG00000108865	<i>Gm44617</i>	0.02	2.52E-05
ENSMUSG00000109136	<i>Gm45114</i>	0.01	1.42E-04

Supplementary Data Table 3 | Deregulated genes in E16.5 *Spocd1*^{-/-} foetal gonocytes.

Table of all statistically significant ($P < 0.01$, Benjamini-Hochberg adjusted two-sided Wald's test), de-regulated (>2 -fold) genes identified in E16.5 *Spocd1*^{-/-} gonocytes, listing fold-change of expression (relative to wildtype) and P-values as determined from RNA-seq data. $n=3$ for both genotypes.

Supplementary Table 4

protein.ID	protein	gene	P-value	fold-enrichment
Q7M739	TPR	<i>Tpr</i>	4.2E-08	239.9
B1ASB6	SPOCD1	<i>Spocd1</i>	6.8E-06	516.5
Q61142	SPINDLIN	<i>Spin1</i>	1.2E-05	93.6
Q3U7Z6	PGAM1	<i>Pgam1</i>	2.1E-05	10.5
H3BKT1	C19ORF84H	<i>Gm38999</i>	3.3E-05	38.7
A2AH22	AMBRA1	<i>Ambra1</i>	3.8E-05	4.5
A2BH40	ARID1A	<i>Arid1a</i>	5.2E-05	7.4
A3EWM2	DNMT3L	<i>Dnmt3l</i>	7.2E-05	5.3
H7BWX9	SUMO2	<i>Sumo2</i>	7.3E-05	39.4
P83917	CBX1	<i>Cbx1</i>	1.0E-04	16.6
Q3U3A7	MTA3	<i>Mta3</i>	1.4E-04	12.3
Q8R2N0	TAP26	<i>Ccdc59</i>	1.8E-04	5.1
Q8BKC5	IMPORTIN5	<i>Ipo5</i>	1.8E-04	6.2
A1L3S7	GATAD2B	<i>Gatad2b</i>	1.8E-04	4.2
Q91ZW3	SMARCA5	<i>Smarca5</i>	1.8E-04	18.0
A0A0R4J2B6	RBBP5	<i>Rbbp5</i>	2.5E-04	7.0
Q544H8	ZBTB14	<i>Zbtb14</i>	2.5E-04	5.1
O88508	DNMT3A	<i>Dnmt3a</i>	3.2E-04	4.4
Q60520	SIN3A	<i>Sin3a</i>	3.4E-04	9.7
E9Q6R4	ARID1B	<i>Arid1b</i>	3.6E-04	11.9
E9Q9N6	MARK2	<i>Mark2</i>	4.5E-04	4.5
Q8K284	GTF3C1	<i>Gtf3c1</i>	4.8E-04	4.3
Q9R190	MTA2	<i>Mta2</i>	6.9E-04	7.1
Q9DCT6	BAP18	<i>Bap18</i>	1.1E-03	5.9
E9QAS4	CHD4	<i>Chd4</i>	1.2E-03	5.1
F8WHY8	MTA1	<i>Mta1</i>	1.2E-03	8.7
O88574	SAP30	<i>Sap30</i>	1.2E-03	4.2
Q3TKT4	BRG1	<i>Smarca1</i>	1.5E-03	7.0
P09411	PGK1	<i>Pgk1</i>	1.5E-03	4.1
Q9Z2D8	MBD3	<i>Mbd3</i>	1.6E-03	4.4
P24549	RALDH1	<i>Aldh1a1</i>	1.7E-03	5.5
Q99MX1	USP26	<i>Usp26</i>	1.7E-03	4.7
Q9CU65	ZMYM2	<i>Zmym2</i>	1.9E-03	5.2
A0A1W2P7G2	SARNP	<i>Sarnp</i>	2.1E-03	4.3
Q923G2	RPABC3	<i>Polr2h</i>	2.1E-03	5.3
Q6DID5	MUM1	<i>Mum1</i>	2.3E-03	4.9
Q99JR8	SMARCD1	<i>Smarcd2</i>	2.4E-03	5.3
Q5EBQ2	PEBP1	<i>Pebp1</i>	2.5E-03	6.5
Q921I1	Serotransferrin	<i>Tf</i>	2.7E-03	6.5
Q6ZWM8	PPP1CC	<i>Ppp1cc</i>	3.1E-03	5.1
Q62383	SPT6	<i>Supt6h</i>	4.7E-03	8.6
Q6URW6	Myosin14	<i>Myh14</i>	5.2E-03	4.6
A0A1D5RLL4	TRRAP	<i>Trrap</i>	5.9E-03	5.6
G3X9B1	HEAT1R1	<i>Heatr1</i>	7.8E-03	5.2
A8DUK2	beta-globin	<i>Hbbt1</i>	8.1E-03	8.5
A2AQ25	SKT	<i>Skt</i>	8.3E-03	4.7
Q8CFG0	SULF2	<i>Sulf2</i>	8.7E-03	4.4
Q58E49	HDAC1	<i>Hdac1</i>	9.2E-03	6.5
Q3ULT2	α-ACTININ4	<i>Actn4</i>	9.4E-03	9.8
P10639	Thioredoxin	<i>Txn</i>	1.0E-02	5.6
O35207	Cdk2ap1	<i>Cdk2ap1</i>	1.1E-02	4.3
P48036	AnxinA5	<i>Anxa5</i>	1.2E-02	4.2
A3KMF2	MKL2	<i>Mkl2</i>	1.2E-02	4.2
Q61103	DPF2	<i>Dpf2</i>	1.2E-02	5.2
A0A140T8S5	CHAMP1	<i>Champ1</i>	1.3E-02	6.0
A0A0N4SVC2	Transformer2A	<i>Tra2a</i>	1.3E-02	4.0
F8VPR5	CREB-BP	<i>Crebp</i>	1.3E-02	4.3
Q9DBJ3	BAIAP2L1	<i>Baiap2l1</i>	1.4E-02	5.5
P15626	GSTM2	<i>Gstm2</i>	1.4E-02	8.6
Q6IRU2	α4-Tropomyosin	<i>Tpm4</i>	1.5E-02	4.9
Q3UEK9	AHSG	<i>Ahsg</i>	1.8E-02	4.0
Q9JJV2	Profilin2	<i>Pfn2</i>	1.9E-02	4.8
Q61391	Nepriylisin	<i>Mme</i>	1.9E-02	4.6
Q91V38	HSP90B1	<i>Hsp90b1</i>	2.2E-02	6.7
F6VXG5	WT1	<i>Wt1</i>	2.4E-02	4.5
Q3U6E4	PTMA	<i>Ptma</i>	2.5E-02	7.0
Q8C7S2	LIMA1	<i>Lima1</i>	2.6E-02	5.1
Q8CIG3	LSD2	<i>Kdm1b</i>	3.5E-02	4.2
Q9Z103	ADNP	<i>Adnp</i>	3.5E-02	5.7
Q8CGZ0	CHERP	<i>Cherp</i>	3.5E-02	4.5
Q9JI95	CPN10-like	<i>Cpn10-rs1</i>	4.0E-02	4.9
Q3U5S6	Syndecan	<i>Sdc4</i>	4.1E-02	4.5
Q62189	U1-A	<i>Snrpa</i>	4.6E-02	5.6

Supplementary Data Table 4 | Proteins identified as SPOCD1 interactors.

Table listing all statistically significant ($P < 0.05$, two-sided Student's t-test) proteins that are at least 4-fold enriched in the SPOCD1-HA immuno-precipitation.

Supplementary Table 5

protein.ID	protein	gene	P-value	fold-enrichment
Q7M739	TPR	<i>Tpr</i>	4.03E-06	38.15
Q71LX8	HSP90AB1	<i>Hsp90ab1</i>	5.03E-06	6.30
Q8CGT6	MIWI2	<i>Piwil4</i>	5.46E-06	25.37
A0A0R4J086	OLFML3	<i>Olfml3</i>	6.13E-06	10.24
Q80Y52	HSP90AA1	<i>Hsp90aa1</i>	1.21E-05	18.25
Q91XW8	FKBP6	<i>Fkbp6</i>	1.29E-05	4.91
A0A0A6YWX1	USP19	<i>Usp19</i>	1.49E-05	17.88
D3YWG8	MOV10L1	<i>Mov10l1</i>	1.89E-05	24.23
Q4FJN2	FKBP5	<i>Fkbp5</i>	2.61E-05	11.96
P30416	FKBP4	<i>Fkbp4</i>	2.95E-05	24.28
Q3THQ5	STIP1	<i>Stip1</i>	2.98E-05	58.52
B2RQL4	ADAD2	<i>Adad2</i>	3.22E-05	18.59
A0A0N4SVL9	PPP6C	<i>Ppp6c</i>	4.33E-05	6.96
Q8BY87	USP47	<i>Usp47</i>	4.68E-05	17.67
Q99MV1	TDRD1	<i>Tdrd1</i>	5.66E-05	5.22
Q8CI32	BAG5	<i>Bag5</i>	7.43E-05	14.63
D3YUE6	GTSF1	<i>Gtsf1</i>	8.63E-05	18.64
Q99MV7	RNF17	<i>Rnf17</i>	9.59E-05	22.21
B1ASB6	SPOCD1	<i>Spocd1</i>	1.77E-04	51.36
F8VPN2	TEX15	<i>Tex15</i>	1.87E-04	11.01
Q14DK4	GPAT2	<i>Gpat2</i>	1.98E-04	13.89
Q3U7Z6	PGAM1	<i>Pgam1</i>	2.48E-04	9.76
P47810	WEE1	<i>Wee1</i>	3.17E-04	4.50
Q8CAE2	HENMT1	<i>Henmt1</i>	4.53E-04	19.48
A6H5Y3	Methione Synthase	<i>Mtr</i>	5.02E-04	10.18
Q99PT1	Rho-GDI1	<i>Arhgdia</i>	5.06E-04	9.31
H3BKT1	C19ORF84H	<i>Gm38999</i>	5.45E-04	5.79
Q8N7N5	DCAF8	<i>Dcaf8</i>	6.01E-04	7.26
Q61142	SPINDLIN	<i>Spin1</i>	6.03E-04	10.48
A0A0G2JFB2	TDRKH	<i>Tdrkh</i>	7.22E-04	22.08
F7BX26	PPP5C	<i>Ppp5c</i>	9.41E-04	4.58
P62311	LSM3	<i>Lsm3</i>	9.97E-04	4.65
M0QWY0	EMC8	<i>Emc8</i>	1.09E-03	5.94
Q8VDN2	ATP1A1	<i>Atp1a1</i>	1.48E-03	4.58
D3Z7C6	PTGES3	<i>Ptges3</i>	1.60E-03	22.20
Q569Z6	THRAP3	<i>Thrap3</i>	1.65E-03	4.53
Q6P5H2	NESTIN	<i>Nes</i>	2.03E-03	5.52
Q9R0P9	UCHL1	<i>Uchl1</i>	2.64E-03	5.37
P83917	CBX1	<i>Cbx1</i>	2.71E-03	7.13
Q8VD46	GASZ	<i>Asz1</i>	2.82E-03	14.61
P02104	HemoglobinY2	<i>Hbby2</i>	2.83E-03	5.97
Q4KL76	HSPE1	<i>Hspe1</i>	3.19E-03	8.76
Q3ULT2	α-ACTININ4	<i>Actn4</i>	4.27E-03	7.74
Q62383	SPT6	<i>Supth6</i>	4.85E-03	5.34
Q80TU6	ACIN1	<i>Acin4</i>	4.91E-03	4.88
Q91ZW3	SMARCA5	<i>Smarca5</i>	5.57E-03	4.79
Q3UI98	GTF3C5	<i>Gtf3c5</i>	7.30E-03	4.36
Q92111	Serotranferrin	<i>Tf</i>	8.15E-03	7.05
Q3TYJ0	STUB1	<i>Stub1</i>	8.75E-03	7.08
A2BH40	ARID1A	<i>Arid1a</i>	9.09E-03	6.79
Q3U3A7	MTA3	<i>Mta3</i>	1.27E-02	5.05
A0A140T8S5	CHAMP1	<i>Champ1</i>	1.31E-02	5.02
Q6IRU2	α4-Tropomyosin	<i>Tpm4</i>	1.75E-02	6.17
P27661	H2AX	<i>H2afx</i>	1.77E-02	11.48
Q5EBQ2	PEBP1	<i>Pebp1</i>	1.92E-02	7.31
Q14AI7	COPS4	<i>Cops4</i>	1.99E-02	4.02
B2RSN3	β-TUBULIN	<i>Tubb2b</i>	2.24E-02	4.47
Q5SUE7	ADAD1	<i>Adad1</i>	2.33E-02	6.57
A2AQ25	SKT	<i>Skt</i>	2.34E-02	5.02
P10649	GSTM1	<i>Gstm1</i>	2.36E-02	5.12
Q80ZK9	WDTC1	<i>Wdtd1</i>	2.47E-02	6.27
Q3UF95	BAG6	<i>Bag6</i>	2.87E-02	4.52
P14733	LAMIN-B1	<i>Lmnb1</i>	3.07E-02	21.48
Q80X90	FilaminB	<i>Flnb</i>	3.27E-02	4.10
Q8BT07	CEP55	<i>Cep55</i>	3.50E-02	4.22
A0A1B0GSX7	NUP98	<i>Nup98</i>	3.61E-02	4.50
Q91V38	HSP90B1	<i>Hsp90b1</i>	3.98E-02	9.58
Q3U6E4	PTMA	<i>Ptma</i>	4.21E-02	4.24
P40142	Transketolase	<i>Tkt</i>	4.39E-02	5.42
Q62189	U1-A	<i>Snrpa</i>	4.98E-02	4.29

Supplementary Data Table 5 | Proteins identified as MIWI2 interactors using benzonase for protein extraction.

Table listing all statistically significant ($P < 0.05$, two-sided Student's t-test) proteins that are at least 4-fold enriched in the HA-MIWI2 immuno-precipitation.

Supplementary Table 6

protein.ID	protein	gene	complex	P-value	fold-enrichment
Q9Z2D8	MBD3	<i>Mbd3</i>	NURD	0.003	2.55
Q9R190	MTA2	<i>Mta2</i>	NURD	0.006	3.51
E9Q6R4	ARID1B	<i>Arid1b</i>	BAF	0.008	3.10
E9QAS4	CHD4	<i>Chd4</i>	NURD	0.009	2.50
F8WHY8	MTA1	<i>Mta1</i>	NURD	0.023	3.19
A3EWM2	DNMT3L	<i>Dnmt3l</i>	DNMT3	0.032	1.94

Supplementary Data Table 6 | Additional NURD, BAF and *de novo* methylation components identified in the MIWI2 IP-MS that used benzonase for protein extraction.

Table listing statistically significant ($P < 0.05$, two-sided Student's t-test) but less than 4-fold enriched proteins from the NURD, BAF and *de novo* methylation machinery complexes co-purified in the HA-MIWI2 IPMS.

Supplementary Table 7

sample.ID	total read count	duplicated reads (removed)	duplication rate [%]	mean read length	total read length	fold coverage	conversion rate [%]
WT_1	74,950,362	5,623,257	6.98	111	24,913,208,414	9.14	99.06
WT_2	57,568,270	3,845,611	6.26	110	18,978,827,940	6.96	98.93
WT_3	43,149,146	3,102,389	6.71	110	14,222,296,134	5.22	99.10
Spocd1_1	67,538,386	4,600,180	6.38	112	22,682,079,257	8.32	98.96
Spocd1_2	52,572,930	3,622,534	6.45	108	17,040,648,058	6.25	98.95
Spocd1_3	47,609,543	3,204,297	6.31	108	15,478,149,570	5.68	99.05
Miwi2_1	68,500,420	5,295,444	7.18	111	22,785,333,541	8.36	99.01
Miwi2_2	61,952,244	4,576,972	6.88	111	20,702,606,662	7.60	99.14
Miwi2_3	66,368,499	4,948,138	6.94	112	22,339,543,890	8.20	99.09

Supplementary Data Table 7 | Sequencing statistics of Methyl-seq datasets

Table listing sequencing and alignment statistics for the Methyl-seq libraries.